

**THE DEVELOPMENT OF A MARGARITE–CORUNDUM BLACKWALL
BY METASOMATIC ALTERATION OF A SLICE OF MICA SCHIST
IN ULTRAMAFIC ROCK, KVESJÖEN, NORWEGIAN CALEDONIDES**

KURT BUCHER[§]

Institute of Mineralogy, Petrology and Geochemistry, University of Freiburg, Albertstr. 23b, D–79104 Freiburg, Germany

CHRISTIAN DE CAPITANI[§]

Mineralogisch-Petrographisches Institut, University of Basel, Bernoullistr. 30, CH–4056 Basel, Switzerland

RODNEY GRAPES

Institute of Mineralogy, Petrology and Geochemistry, University of Freiburg, Albertstr. 23b, D–79104 Freiburg, Germany

ABSTRACT

An unusual occurrence of blackwall rock occurs on a promontory in Lake Kvesjöen, in the Norwegian Caledonides, at the contact between a lens of ultramafic rock (Fo–En-rock) 200 m in diameter and amphibolite-facies metapelitic country-rocks. The blackwall contains corundum, staurolite, tourmaline and four micas: muscovite, paragonite, margarite and biotite. Accessories include allanite–epidote, apatite, ilmenite, rutile, monazite, and zircon. The blackwall evolved from a normal quartz-rich staurolite–garnet–biotite metapelite by progressive loss of SiO₂ to the silica-deficient Fo-rich ultramafic rock at about 570°C and 6.5 kbar. Thermodynamic modeling of the metasomatic process predicts first the disappearance of garnet and excess quartz, and then the production of corundum from excess Al₂O₃. Subsequent desilication of plagioclase then results in the formation of paragonite and margarite in addition to the “primary” muscovite and biotite. Abundant development of biotite at the expense of staurolite and muscovite at a late stage of the process leads to the observed dark biotite-rich corundum–margarite rock. The model process predicts the observed blackwall mineralogy and also suggests that the corundum–margarite rock represents a mature end-product of the metasomatic reaction. The SiO₂ lost by the metapelite reacted with forsterite and enstatite of the ultramafic rock to form talc. The chemical potential of SiO₂ imposed by the talc–forsterite assemblage was much lower than that given by quartz saturation in the metapelite under the prevailing conditions during the active process. The resulting gradient in chemical potential was the prime driving force in the formation of the blackwall.

Keywords: blackwall, metasomatism, margarite, corundum, ultramafic rocks, desilication, Lake Kvesjöen, Norwegian Caledonides.

SOMMAIRE

Nous signalons un exemple inhabituel de “paroi noire” sur un promontoire dans le lac Kvesjöen, dans les Calédonides norvégiennes, au contact entre une lentille de roche ultramafique (roche à Fo–En) d’un diamètre de 200 m et un encaissant métapélitique (faciès amphibolite). La paroi noire contient corindon, staurolite, tourmaline et quatre micas: muscovite, paragonite, margarite et biotite. Parmi les accessoires, on trouve allanite–épidote, apatite, ilménite, rutile, monazite, et zircon. Cette paroi noire s’est formée à partir d’une métapélite banale à staurolite – grenat – biotite et riche en quartz par perte progressive de SiO₂ à la roche ultramafique adjacente, riche en Fo et déficitaire en silice, à environ 570°C et 6.5 kbar. Un modèle thermodynamique du processus métasomatique prédit d’abord la disparition du grenat et de l’excédent de quartz, et ensuite la production de corindon à partir de l’excédent en Al₂O₃. Une désilication subséquente du plagioclase a donné lieu à la formation de paragonite et de margarite, ajoutées à la muscovite et la biotite “primaires”. Un développement tardif et abondant de biotite aux dépens de staurolite et de muscovite a donné l’aspect sombre de la roche à corindon–margarite. Le modèle prédit la minéralogie observée de la paroi noire et mène à l’hypothèse que la roche à corindon–margarite représente un terme stable de la réaction métasomatique. La silice perdue par la métapélite a réagi avec la forstérite et l’énstatite de la roche ultramafique pour former du talc. Le potentiel chimique de SiO₂ fixé par l’assemblage talc–forstérite était largement inférieur au niveau établi par la métapélite saturée en quartz au cours du processus aux conditions préconisées. Le gradient en potentiel chimique qui en résulta était le moteur principal de formation de la paroi noire.

(Traduit par la Rédaction)

Mots-clés: paroi noire, métasomatose, margarite, corindon, roches ultramafiques, désilication, lac Kvesjöen, Caledonides norvégiennes.

[§] *E-mail addresses:* bucher@uni-freiburg.de, christian.decapitani@unibas.ch

INTRODUCTION

The occurrence of forsterite-rich mantle rocks as pods and lenses is common in many orogenic belts. These so-called Alpine-type peridotites reflect deep mechanical crust–mantle interaction during subduction, nappe stacking and later exhumation (Coleman 1971, Chidester & Cady 1972, Lockwood 1972, Evans 1977, Stigh & Ronge 1978, Bucher-Nurminen 1991). The ultramafic rocks commonly form solitary and isolated bodies of tens to some hundreds of m in length. Rare occurrences may even be a few km in size.

Dark bands or zones mostly consisting of biotite occur commonly at the contacts between such Alpine-type ultramafic bodies and the quartzofeldspathic rocks of the envelope. The bands are soft and black masses of biotite and are consequently called *blackwall*. The thickness of the blackwalls is variable, but typically the zones are some tens of cm thick. Depending on the metamorphic conditions during blackwall formation, chlorite or amphibole and other minerals may be part of the blackwall assemblage. Many well-documented field studies of blackwall occurrences (*e.g.*, Read 1934, Phillips & Hess 1936, Matthews 1967, Curtis & Brown 1969, Griffin 1971, Frost 1975, Cooper 1976, Evans 1977, Sharpe 1980, Sanford 1982, Peacock 1987, Grapes & Palmer 1996, Puschignig 2002, Dubinska & Wiewióra 1999, Takla *et al.* 2003) have shown that these exceptional rocks typically developed systematic zoned sequences of assemblages at the contact between rocks of contrasting compositions. Therefore, the investigators concluded that blackwalls form as result of chemical potential gradients and diffusive mass-transfer of major rock-forming components across the contact. In a classic paper, Thompson (1959) showed that a simple predictable zoned sequence of reaction products will develop at the contact of dunite (forsterite) and quartzite (quartz) by a process called bimetasomatism, diffusion of Si toward the ultramafic rock and Mg toward the felsic rock.

However, blackwall formation may also involve infiltration metasomatism and mass transfer by fluid flow. It has also been shown in most field studies (for a selection of references, see above) that the contacts between bodies of ultramafic rocks and their envelope are tectonic in nature, and the sheared faults along the contact are preferred paths of migration for fluid flow. Blackwall formation is thus the result of combined infiltration – diffusion metasomatism, with a component of fluid flow parallel to the contact and a diffusive flux normal to the contact, with clear evidence for the importance of mass transfer in rock-forming processes in general (*e.g.*, Curtis & Brown 1969, Frost 1975).

The mineral zonation that develops in the blackwall depends on metamorphic grade at which the metasomatic process takes place and on the rock type forming the envelope of the ultramafic body. However, shells of chlorite and particularly biotite are the most common.

In the lower- and middle-amphibolite facies, an ideal zonal sequence through a contact zone between an ultramafic rock and gneiss may consist of: biotite gneiss / quartz-free gneiss / mica-rich gneiss / biotite shell (blackwall) / actinolite – chlorite – biotite rock / actinolite – chlorite – talc rock / talc – forsterite rock (*e.g.*, Winter 2001). Under lower-grade, greenschist-facies conditions, chlorite may be the only blackwall sheet silicate. However, muscovite-rich zones commonly form in desilicated quartzofeldspathic rocks near the contact (*e.g.*, Koons 1981).

In this study, we present information on blackwall rocks with an unusual mineralogy that evolved from a slab of garnet – staurolite – biotite schist wedged into a body of ultramafic rock. The metasomatic process transformed the primary schist into a desilicated corundum-rich residue. The focus of the investigation is on the reactions and mineralogical changes that accompany the step-wise transformation of one rock into the other. The principal questions include: what kind of specific processes lead to the development of minerals not originally present in the unaltered rock, and what are the driving forces for component migration in quantitative terms. Finally, we attempt to thermodynamically model the development of Al-rich blackwall quantitatively in order to predict the succession of assemblages in the altered rock and to evaluate the preserved state of the metasomatic process.

REGIONAL GEOLOGICAL SETTING

The blackwall rocks of this study were collected from a small promontory in Kvesjöen, a lake of the Nordli district, east of Grong, about 200 km north of Trondheim, Norway (Fig. 1). The precise locality is Storhamaren (map sheet Murusjöen 1:50000, 1923–I, coordinates 51.4/47.9). The promontory is composed of ultramafic rock and at the lakeshore of Kvesjöen there is an exposed outcrop of blackwall and the contact with the unaltered mica schist.

The rock association at the Storhamaren outcrop is part of the Upper Allochthonous Unit of the Scandinavian Caledonides (Fig. 1) (Roberts & Gee 1985, Gee *et al.* 1985). This stack of far-traveled nappes can be further divided into a lower series of nappes, the Seve nappes, and an upper series of nappes, the Köli nappes (not distinguished in Fig. 1). The contact of the Köli and Seve nappes is a major thrust fault that occurs immediately west of the Kvesjöen locality (Fig. 2). The investigated occurrence of blackwall rock is part of the lower unit, the Seve nappes of the Upper Allochthonous Unit (Fig. 2). Mica schist and gneiss dominate this supracrustal unit. In addition to the aluminous metasedimentary units, minor amounts of quartzite and marble occur in the sequence. The felsic rocks are locally migmatized further to the east. Extensive areas of outcrop within the unit are composed of amphibolite. The mafic rocks are of igneous origin, but now have an

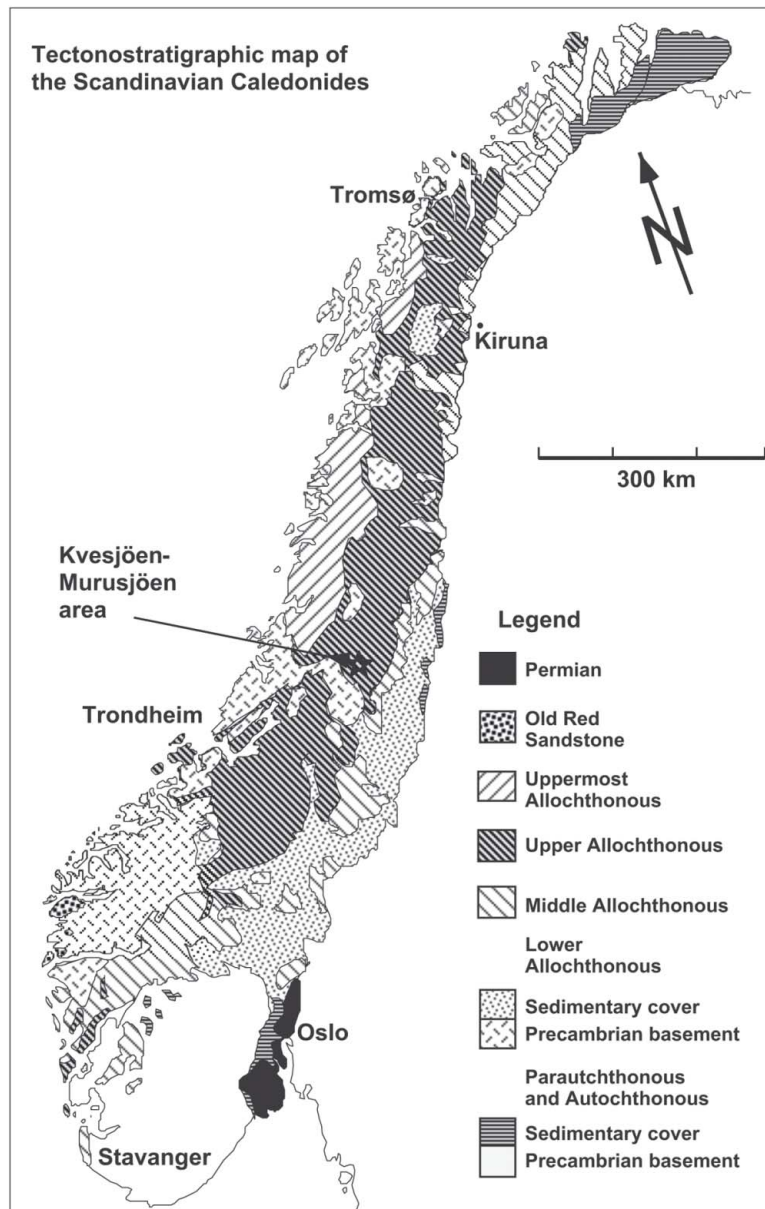


FIG. 1. Geological map of Norway (Roberts & Gee 1985) showing the blackwall locality at Kvesjöen–Murusjöen described in this paper. Note that the locality is in the Seve Nappes of the Upper Allochthonous Unit, which are not distinguished from the tectonostratigraphically higher Köli Nappes in the western part of the Upper Allochthonous Unit (Fig. 2).

amphibolite-facies assemblage. The mica schist contains, in addition to biotite, muscovite, plagioclase and quartz, staurolite, garnet, and occasionally kyanite. The assemblages of amphibolites and metapelites imply

metamorphic conditions of approximately 600°C and 7 kbar (Bucher & Frey 2002). Toward the Köli Thrust, the metamorphic grade decreases slightly, and migmatitic textures are absent in the study area. The

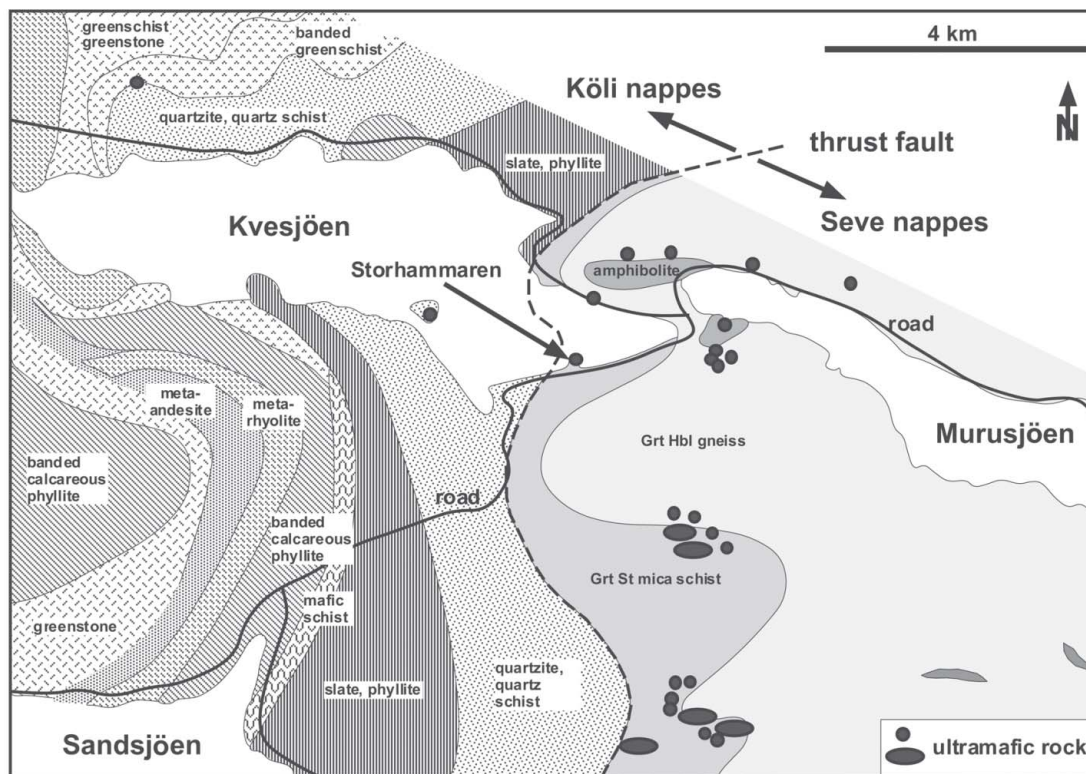


Fig. 2. Geological map of the Kvesjöen–Murusjöen area (Foslie 1959, Sigmond *et al.* 1984) showing the units of the Upper Allochthonous (Fig. 1). Note the abundance of outcrops of ultramafic rocks along the major thrust fault between the Seve and Köli nappes within the Upper Allochthonous Unit. Blackwall locality: Storhammaren (Fig. 3).

Seve unit is overthrust by the Köli nappes (Fig. 2), an extensive stack of low-grade thrust sheets containing flysch-type metasedimentary rocks and ophiolite with greenschist-facies serpentinites (Bucher-Nurminen 1991).

A distinct feature of the area is the occurrence of a large number of isolated Alpine-type peridotites in the Upper Allochthon (Qvale & Stigh 1984, Bucher-Nurminen 1988). More than 20 ultramafic bodies greater than 50 m in diameter occur in the immediate Kvesjöen–Murusjöen area (Fig. 2). The ultramafic rocks are concentrated along the main thrust separating the Seve and Köli nappes within the Upper Allochthonous Unit. The close spatial relationship of ultramafic rocks to major thrust faults in the Scandinavian Caledonides in general suggests that the ultramafic rocks represent fragments of mantle tectonically emplaced along the zones of major thrust separating the crustal stacks of nappes (Bucher-Nurminen 1991). All the ultramafic rocks are of the same metamorphic grade as the host gneiss and schist (Bucher-Nurminen 1988). The isofacial nature of the ultramafic rocks shows that re-

gional amphibolite-facies metamorphism overprinted the ultramafic bodies after their emplacement.

THE BLACKWALL OUTCROP

The Storhammaren ultramafic body (Fig. 3) measures about 200 m in diameter and is well exposed along the shore of Kvesjöen. The yellow-brown outcrop of coarse-grained peridotite is in contact with marble and amphibolite to the east and with garnet mica schist to the west. Along the western contact, a thin (~20 cm) biotite-rich blackwall separates the mica schist from peridotite (locality A, Fig. 3). About 40 m from the contact, a thin zone or band of mica schist and gneiss occurs within the peridotite (locality B, Fig. 3). The site of the outcrop suggests that the slab of finely banded schist and gneiss has been tectonically wedged into the peridotite. Biotite-rich blackwall rocks are present at locality B; they contain conspicuous cm-size crystals of corundum. All blackwall samples described in this paper are from locality B. The samples of unaltered mica schist have been collected from locality A, about 4 m

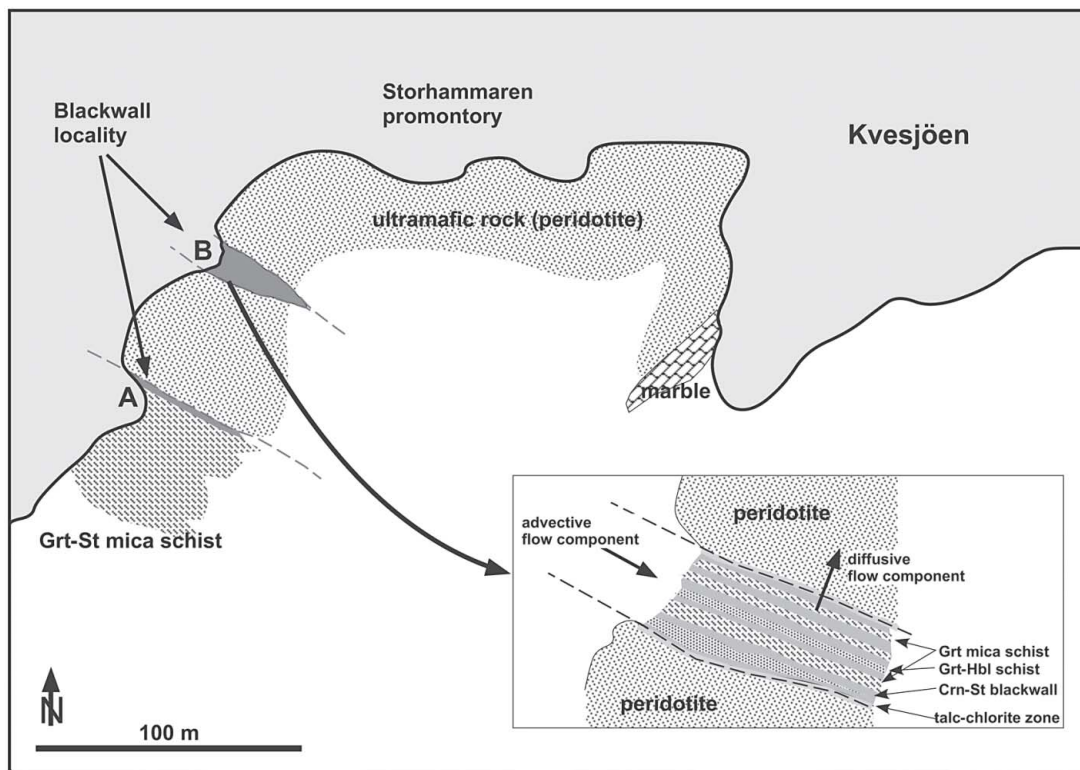


FIG. 3. Outcrop map showing the blackwall association at Storhammaren, a promontory in the lake Kvesjøen. The geological position of the outcrop within the Scandinavian Caledonides is given in Figures 1 and 2. Samples of unaltered mica schist were collected at locality A, and blackwall rock samples, from locality B.

from the contact (*e.g.*, KB1006). At locality B, an irregularly banded sequence of mica schist is exposed (Fig. 3). The felsic rocks show diverse extents of metasomatic alteration, and the banding is roughly parallel to the contacts to the peridotite. The immediate contact with the peridotite consists of a thin zone (a few cm) of chlorite and talc. The altered mica schist varies from garnet-bearing but quartz-free staurolite-garnet schist (sample KB1003, KB1004, KB1005) to corundum-bearing staurolite-biotite schist (samples KB298, KB1002) and corundum-rich biotite schist (KB299, KB1001). The irregular distribution of the blackwall rocks at locality B (Fig. 3) excludes simple diffusion-induced metasomatism (bimetasomatism) with mass transfer normal to the schist-peridotite contact as the exclusive rock-forming process. The field situation at locality B rather suggests that fluid advection parallel to the schist wedge was an important component of the alteration process.

PETROGRAPHY

Ultramafic rocks

Outcrops of ultramafic rocks are conspicuous because of their yellow to brown weathering rinds and lack of vegetation cover. Nine samples from four outcrops have been examined microscopically. Earliest-generation minerals includes very large and deformed relict forsterite and, in a few samples, enstatite. All other minerals are texturally younger than the Fo + En assemblage. Chlorite and talc are ubiquitous in all samples. Tremolite and cummingtonite are modally abundant in several samples. The assemblages and modal compositions are typical of amphibolite-facies lherzolites (Evans 1977). Very late in the reaction-recrystallization history of many of the rocks, minor antigorite formed together with small amounts of magnetite, with the antigorite epitactically overgrowing chlorite of the amphibolite-facies assemblage.

The randomly oriented flakes of talc cross-cutting fractured euhedral crystals of forsterite suggest the replacement of forsterite by talc (Figs. 4a, b). This reaction requires the introduction of a silica-rich aqueous fluid. Similar textures suggest an analogous replacement of enstatite by talc. Such replacement of forsterite and enstatite is pervasive and not restricted to the outer zones of the ultramafic bodies. Subhedral tremolite occurs with chlorite (Fig. 4c). Very minor amounts of antigorite formed in the terminal phase of the reaction history. Its scarcity reflects minor retrogradation during cooling.

Although the textures shown in Figure 4 clearly demonstrate forsterite resorption and its replacement by talc, forsterite forms a stable assemblage with talc (Fig. 4d). Talc is both an alteration product of forsterite resorption and in equilibrium with forsterite at the same time. The reaction $\text{forsterite} + \text{SiO}_{2\text{aq}} + \text{H}_2\text{O} \Rightarrow \text{talc}$ is an equilibrium reaction; it stops when the supply of externally derived $\text{SiO}_{2\text{aq}}$ ceases, leaving the stable assemblage Fo

+ Tlc in the rock. The chemical potential of SiO_2 is then controlled and defined by the ultramafic rock, specifically by the assemblage Fo + Tlc in the presence of H_2O (for more details, see below).

The absence or scarcity of magnesite in the alteration assemblage is important and unusual in view of other occurrences of ultramafic rocks in the Scandinavian Caledonides (Bucher-Nurminen 1988). Magnesite does occur as a minor phase in some samples, indicating that the fluid was poor in CO_2 . The stable assemblage at the peak of the regional amphibolite-facies metamorphism was forsterite + talc + chlorite + tremolite, with talc largely predominant over tremolite.

Mica schists

Mica schists have a variable mineralogy and bulk composition. The most common rock is a garnet-staurolite mica schist. It contains more than 15% quartz and

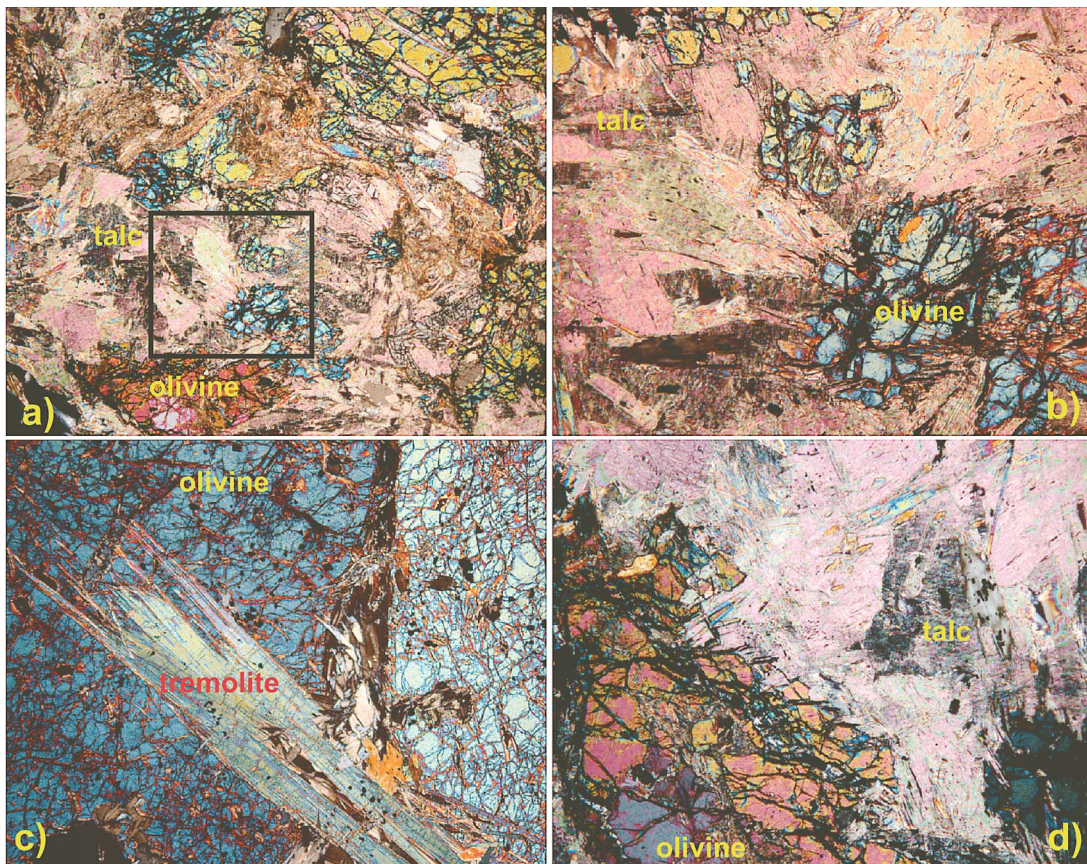


FIG. 4. Photomicrographs of textures in ultramafic rocks: a) replacement of olivine by talc, frame area of b) detailed texture of olivine dissolution and replacement by talc, c) tremolite growth by reaction of olivine with fluid, d) resorption of olivine by SiO_2 metasomatism. Width of field of view: a and c: 4 mm, b and d: 1 mm; crossed polarizers.

about 20–30% feldspar. Euhedral porphyroblasts of staurolite (up to 5 mm) make up about 10–15% of the rock; also present are garnet (10%), biotite (20%) and chlorite (10%). Chlorite appears to be a part of the main assemblage. Small grains of tourmaline constitute several percent of the rock. White mica is scarce; in some samples, muscovite and paragonite are present in small amounts. The mica schist is a typical metapelite of the lower- to middle-amphibolite facies, and the AFM configuration is shown in Figure 5. The main-stage metamorphic assemblage is $Qtz + Pl + Bt + Grt + St + (Chl) \pm Ms$ (Figs. 6a, b) (all abbreviations after Kretz 1983).

Samples of mica schist, collected at the blackwall outcrop (e.g., KB1005, locality B, Fig. 3), show the same appearance and field aspect as the samples from locality A outside the ultramafic body. However, the samples are devoid of quartz and contain significantly more biotite (30–40%) than mica schist of the envelope. A new generation of fine-grained and euhedral staurolite is present (Fig. 6c). The rocks also contain texturally late muscovite (Fig. 6c) and some kyanite. The textural features suggest that the metasomatic process has modified the mica schist at locality B.

Blackwall rocks

Sample KB298 is a representative sample of a finer-grained, dark gray, less biotite-rich metasomatized mica schist of the blackwall assemblage. The rock consists of biotite (30%), muscovite (20%) intergrown with minor paragonite, and staurolite (20%) as major constitu-

ents. Strongly corroded staurolite porphyroblasts are coarse (mm sized) and resemble the staurolite of the inferred mica schist protolith (Fig. 7a). The texture suggests that staurolite has been dissolving in late blackwall-forming reactions. Euhedral corundum with a blue core is present as randomly oriented crystals some mm across. Paragonite occurs in two textures: a) associated with muscovite in an arrested reaction relationship, as indicated by patchy, corroded grain outlines within muscovite (see below in Mineral Compositions), and b) as texturally late randomly oriented grains overgrowing matrix biotite (Fig. 7b). Large (mm-sized) blades of margarite (>5%) cross-cut and overgrow matrix biotite, indicating late formation of the mica (Fig. 7c). Margarite and paragonite formed at late stages of the blackwall-forming process. Biotite of the matrix is randomly oriented and was also formed by the blackwall-forming process (Fig. 7c). A few grains of kyanite (1–2 mm), with an irregular outline indicating resorption, occur intergrown with muscovite and margarite, but also are present as strongly resorbed grains in staurolite. The kyanite textures are very similar to the occurrence of kyanite in the altered mica schist (KB1005). We interpret kyanite as an intermediate product that formed at early stages of alteration of the mica schist protolith. Blue-green tourmaline is characterized by abundant inclusions of margarite, fine-grained kyanite, and rare biotite and muscovite. Rutile, ilmenite, apatite, zircon, epidote–allanite (Fig. 7b), rare specks of xenotime, and monazite (partly reacted to apatite, chlorite and thorite) are accessories.

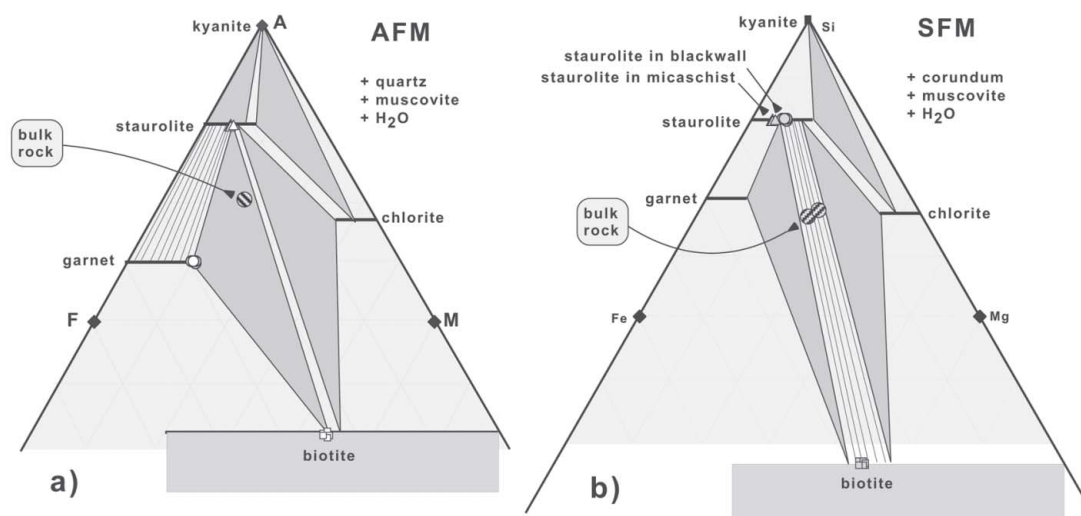


FIG. 5. a) AFM diagram of assemblages in mica schists; the prominent rock type contains the assemblage $Grt + Bt + St + Pl + Chl + Ms + Qtz$; bulk rock KB1006 and mineral compositions are shown. b) SFM projection of rock and mineral compositions of KB298 and KB299 from excess corundum and muscovite.

Blackwall sample KB299 is a black biotite-rich rock containing large, cm-sized crystals of corundum, coarse staurolite, tourmaline and three white micas (paragonite, margarite and muscovite). Randomly oriented mm-sized biotite represents more than 40 vol.% of the rock. As in sample KB298, biotite formed after the last penetrative deformation, and it is the main product of blackwall formation. Also, the corundum crystals (about 25 vol.%) are randomly oriented and developed late, after deformation (Fig. 7d). It is not present in the mica schist and gneiss envelope of the ultramafic body. Thus corundum grew together with biotite after the last major phase of deformation. The occurrence and texture of staurolite in this sample are similar to those in sample KB298, supporting an explanation as corroded relic from the mica schist. A few grains of resorbed kyanite are present, but its textural status is somewhat uncertain. The grains are texturally very similar to resorbed kyanite in the altered mica schist (KB1005). Thus it is interpreted as being relic from an intermediate stage of the blackwall-forming process. Muscovite is a minor phase in this sample (~5%). Paragonite and margarite both are late and occur in similar textures as in sample KB298. Both micas occur in equal amounts, about 10 vol.%. Large crystals of essentially unzoned tourmaline contain numerous inclusions of biotite. Accessories are rutile, ilmenite, apatite, epidote–allanite, monazite, and zircon.

TABLE 1. COMPOSITION OF THE ROCKS AT KVESJØEN, NORWEGIAN CALEDONIDES

Rock type	Blackwall				Schist ¹	Mica schist
	KB298	KB299	KB1001	KB1002	KB1005	KB1006
Sample	KB298	KB299	KB1001	KB1002	KB1005	KB1006
SiO ₂ wt.%	33.63	26.09	24.51	32.36	46.49	50.95
TiO ₂	1.74	1.59	1.69	1.39	1.17	2.66
Al ₂ O ₃	38.42	45.78	41.47	38.47	25.99	17.65
Fe ₂ O ₃ **	10.54	10.48	11.62	8.64	8.95	12.90
MnO	0.06	0.06	0.08	0.05	0.14	0.29
MgO	6.54	6.47	9.53	5.49	4.87	5.75
CaO	0.58	1.66	1.70	1.26	3.44	3.50
Na ₂ O	0.09	0.90	0.48	1.18	3.74	2.34
K ₂ O	5.30	3.98	5.41	5.15	2.77	2.63
P ₂ O ₅	0.09	0.11	0.22	0.06	0.31	0.69
CO ₂	0.09	0.09				
C	0.02	0.02				
H ₂ O	3.32	3.09				
Total	99.79	99.56	96.71	94.05	97.88	99.36
LOI*	3.27	3.19	1.89	2.76	0.91	0.65
Si	32.28	24.57	23.16	31.53	43.97	49.64
Al	43.48	50.82	46.05	44.27	29.00	20.19
Fe**	7.62	7.43	8.24	6.32	6.37	10.48
Mg	9.36	9.08	13.46	7.94	6.86	8.38
Ca	0.60	1.67	1.72	1.32	3.49	3.63
Na	0.17	1.64	0.88	2.25	6.86	4.22
K	6.49	4.78	6.51	6.37	3.33	3.22
O	150.70	146.77	142.48	149.35	153.26	155.77

¹ Altered quartz-free garnet mica schist. * Loss on ignition adjusted for FeO determination and total Fe difference from total Fe = Fe₂O₃. ** Total Fe as Fe₂O₃. X-ray-fluorescence data.

Rock KB299 is considered to be representative of the most altered version of the original mica schist. In contrast to the original mica schist, none of the blackwall rocks contain garnet. The thermodynamic modeling presented below predicts that garnet of the mica schist is the first mineral that will disappear in the course of the metasomatic process. The main arguments in favor of the garnet–staurolite mica schist being the protolith of the corundum–margarite blackwall are the following: a) staurolite occurs exclusively in the garnet–staurolite mica schist outside the ultramafic rock, b) there is a close spatial association of partly altered mica schist and corundum–biotite rocks at locality B (Fig. 3), c) staurolite contains characteristic epidote–allanite inclusions in both rocks, d) both rocks contain characteristic tourmaline crystals of similar composition, e) garnet–staurolite mica schist is the only rock in the envelope close to the slab of corundum–margarite blackwall (Fig. 3).

CHEMICAL COMPOSITION OF THE BLACKWALL ROCKS

The chemical composition of garnet–staurolite mica schist KB1006 from the envelope of the ultramafic body representing the protolith of the corundum–margarite blackwall (Fig. 3), sample KB1005 representing partially altered mica schist, and the four samples of blackwall rock are given in Table 1 (major elements) and Table 2 (trace elements). The high Si-content of the mica schist contrasts with the low-Si, high-Al attributes of the blackwall rocks (Fig. 8). It follows from the observations presented in the previous sections that the mica schist is the protolith of the margarite–corundum blackwall. The chemical composition of the samples

TABLE 2. TRACE-ELEMENT CONCENTRATIONS IN THE ROCKS FROM KVESJØEN, NORWEGIAN CALEDONIDES

Sample	KB298	KB299	KB1001	KB1002	KB1005	KB1006
Ba ppm	8573	4914	3831	9707	864	484
Cr	126	121	125	101	76	43
Ni	69	61	73	52	63	45
Pb	34	38	44	55	49	13
Rb	167	145	216	157	127	98
Sc	23	17	34	29	21	14
Sr	942	2436	1096	3121	971	166
V	193	196	241	193	92	186
Zn	83	103	87	88	156	553
Zr	316	260	322	206	261	318
C	625	769				
Ce	105	102				
Cl	69	77				
F	753	736				
Ga	28	30	37	33	29	<5
La	169	145				
Nb	31	32	43	54	41	47
Th	20	17	46	42	31	14
U	8	7	19	8	10	3
Y	89	77	113	105	81	44
Cu			7	6	3	4115

X-ray-fluorescence data.

thus shows that the latter represents an Al-rich residuum of the mica schist after extraction of silica. Following Dugald Carmichael's arguments from his classic 1968 paper, the mobility of Al was probably low during blackwall formation as a result of the low solubility of Al-phases in typical crustal fluids (Carmichael 1968). Thus if normalized to constant aluminum, it is evident that both blackwall samples have lost a very high proportion of SiO₂ (Fig. 9). As for the other major oxides, MgO and K₂O (especially in KB298) are slightly enriched, and FeO (total iron) and Na₂O are depleted with respect to the inferred protolith (Table 2, Fig. 9). Other gains and losses are small and somewhat uncertain to quantify because of the large representative volume owing to the coarse-grained nature of the rocks. On the basis of conservation of Al, Ti is conserved as well (Fig. 9), supporting the Al-conservation assumption.

From Figure 9, it follows that the entire process is overwhelmingly dominated by SiO₂ loss. The Al-conservation model invoked here implies that all aluminum of the blackwall sample KB299 (about 46 g per 100 g rock) is inherited from the mica schist; the same amount of Al was contained in 190 g of rock. The mass loss associated with the transformation of mica schist to margarite-corundum blackwall is attributed mostly to the loss of SiO₂ (90% of the mass loss). Fe₂O₃ contributes 8%, and Na₂O, about 2% of the mass loss. Because of similar densities of the two types of rocks, this corresponds to a volume loss of about 50%. Much of this volume loss is compensated by the associated increase in volume of the ultramafic rock, which results from forsterite replacement by talc (Mg-balanced talc-forming reaction corresponds to a 50% volume increase). The blackwall rock gains small amounts of MgO, CaO and K₂O. The total of the mass gain is only 4% of the mass

TABLE 3. COMPOSITIONS OF WHITE MICAS FROM BLACKWALL SAMPLE KB299

	Muscovite						Paragonite						Margarite					
	1	5	6	7	11	12	1	2	3	4	5	6	1	4	5	6	12	13
SiO ₂ wt.%	46.29	44.12	43.72	43.57	43.25	43.25	45.74	45.57	45.54	44.06	45.56	45.37	32.62	32.62	32.77	32.62	31.64	31.38
TiO ₂	0.76	0.42	0.46	0.44	0.40	0.53	0.28	0.27	0.30	0.20	0.29	0.14	0.21	0.19	0.25	0.20	0.17	0.18
Al ₂ O ₃	37.60	36.79	36.02	35.95	36.67	35.97	41.61	41.72	42.26	41.39	41.39	41.30	47.95	48.69	48.31	48.69	49.71	49.62
FeO	1.38	1.73	1.76	1.85	1.82	1.88	0.65	0.70	0.71	0.76	0.94	0.86	0.78	0.84	0.76	0.84	0.69	0.71
MgO	0.67	0.76	0.74	0.67	0.56	0.69	0.11	0.12	0.12	0.14	0.12	0.17	0.42	0.42	0.42	0.42	0.32	0.39
CaO	0.02				0.03	0.02	0.64	0.75	0.54	1.15	0.67	1.83	9.01	9.33	9.45	9.33	9.93	10.52
Na ₂ O	2.13	1.64	1.67	1.73	1.80	1.62	5.32	6.09	5.50	5.64	5.36	4.99	2.65	2.25	2.23	2.25	1.70	1.72
K ₂ O	6.93	6.55	6.75	6.92	6.24	6.15	1.15	1.26	1.35	1.14	1.88	0.83	0.13	0.14	0.13		0.04	0.02
BaO	0.78	2.84	2.93	2.93	3.87	4.03	0.07	0.16	0.14	0.12	0.39	0.46			0.09			
Total	96.56	94.87	94.06	94.06	94.65	94.17	95.61	96.64	96.46	94.60	96.60	95.98	93.77	94.48	94.43	94.35	94.21	94.54
Si <i>apfu</i>	6.03	5.98	6.00	5.99	5.94	5.98	5.82	5.77	5.76	5.70	5.80	5.79	4.38	4.34	4.37	4.35	4.22	4.19
^{IV} Al	1.97	2.02	2.00	2.01	2.06	2.02	2.18	2.23	2.24	2.30	2.20	2.21	3.62	3.66	3.63	3.65	3.78	3.81
^{VI} Al	3.80	3.86	3.83	3.82	3.89	3.85	4.06	4.01	4.07	4.02	4.01	4.01	3.96	3.99	3.96	3.99	4.04	3.99
Ti	0.07	0.04	0.05	0.05	0.04	0.06	0.03	0.03	0.03	0.02	0.03	0.01	0.02	0.02	0.03	0.02	0.02	0.02
Fe	0.15	0.20	0.20	0.21	0.21	0.22	0.07	0.07	0.08	0.08	0.10	0.09	0.09	0.09	0.08	0.09	0.08	0.08
Mg	0.13	0.15	0.15	0.14	0.11	0.14	0.02	0.02	0.02	0.03	0.02	0.03	0.08	0.08	0.08	0.08	0.06	0.08
Ca	0.00	0.00	0.00	0.00	0.00	0.00	0.09	0.10	0.07	0.16	0.09	0.25	1.30	1.33	1.35	1.33	1.42	1.50
Na	0.54	0.43	0.44	0.46	0.48	0.43	1.31	1.50	1.35	1.42	1.32	1.24	0.69	0.58	0.58	0.58	0.44	0.44
K	1.15	1.13	1.18	1.21	1.09	1.09	0.19	0.20	0.22	0.19	0.31	0.14	0.02	0.02	0.02	0.00	0.01	0.00
Ba	0.04	0.15	0.16	0.16	0.21	0.22	0.00	0.01	0.01	0.01	0.02	0.02	0.00	0.00	0.00	0.00	0.00	0.00
X _{Fe}	0.54	0.56	0.57	0.61	0.65	0.60	0.77	0.77	0.77	0.75	0.81	0.74	0.51	0.53	0.50	0.53	0.55	0.51
Mrg	0.16	0.00	0.00	0.00	0.28	0.19	5.50	5.65	4.46	9.05	5.31	15.45	64.54	68.76	69.28	69.62	76.07	77.03
Pg	31.79	27.56	27.33	27.53	30.39	28.53	82.73	83.04	82.25	80.28	76.93	76.21	34.35	30.01	29.58	30.38	23.57	22.79
Ms	68.05	72.44	72.67	72.47	69.33	71.27	11.77	11.31	13.28	10.68	17.75	8.34	1.11	1.23	1.13	0.00	0.36	0.17

Single-point analyses on grains. On back-scattered electron images, lighter grey areas in single grains are more Ba-rich (see Figs. 11, 12, 13). There are trace amounts of Mn, Cr, Cl, and F. Cation proportions, in atoms per formula unit (*apfu*), are calculated on the basis of 22 atoms of oxygen.

loss. Whereas the ultramafic body is an obvious source for MgO, the sources for other components are less apparent. However, all small gains and losses of components other than SiO₂ (and perhaps Fe₂O₃) are probably related to the compositional heterogeneity of the protolith. The samples have not been analyzed for boron; however, the presence of twice as much tourmaline in the blackwall (KB299) compared to the unaltered mica schist suggests that boron has been passively enriched in the blackwall as a result of silica loss of the original mica schist. The major-element data thus show that blackwall formation is essentially a process of silica-loss accompanied by a minor loss of iron, which increased X_{Mg} of the bulk rock.

Abundant biotite (and tourmaline) control the high content of MgO (6.54 and 6.47%) and K₂O (5.30 and 3.98%) in KB298 and 299, respectively. The higher modal proportion of paragonite, margarite and lower modal muscovite in KB299 are reflected in higher Ca

(1.66% CaO), Sr (2436 ppm) and Na (0.90% Na₂O), with lower Ba (4915 ppm) in KB299 compared to KB298 (with 0.58% CaO, 942 ppm Sr, 0.09% Na₂O and 8573 ppm Ba). The carbon content of the blackwall (625 and 769 ppm C; Table 2) is mostly present as CO₂ (0.09%) in fluid inclusions (no carbonate is present), and minor organic carbon as graphite (0.02%) (Table 1), which is consistent with the presence of ilmenite, rutile and low bulk-rock oxidation ratios of 40.9 (KB298) and 27.7 (KB299).

If the trace-element data of the blackwall material (Table 2) are compared with the mica schist on the basis of Al conservation, several elements (Ba, Rb, Sr, F, La, Y and V) are obviously enriched in the blackwall. Barium (and Rb) are found in high concentrations in muscovite and biotite, with muscovite > biotite, and Sr is strongly enriched in margarite, a mineral that is not present in the mica schist. The high F-content of the blackwall rocks (753 and 736 ppm in KB298 and 299,

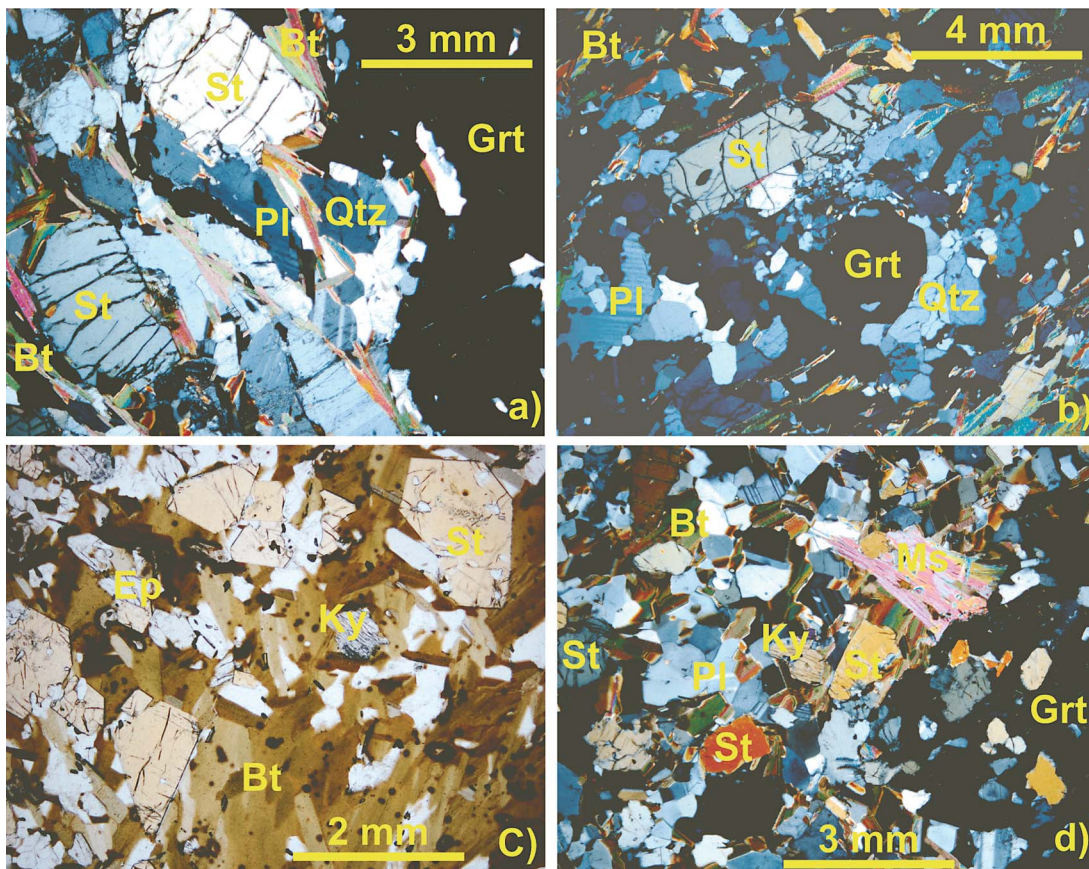


FIG. 6. Photomicrographs of textures in mica schist KB1006: a) St + Grt + Bt + Pl + Qtz, and b) St + Grt + Bt + Pl + Qtz, and in altered Qtz-free mica schist KB1005: c) second generation of euhedral staurolite formed during metasomatism, relict kyanite, and d) development of phengitic muscovite during alteration in assemblage St + Grt + Pl + Bt + Ms.

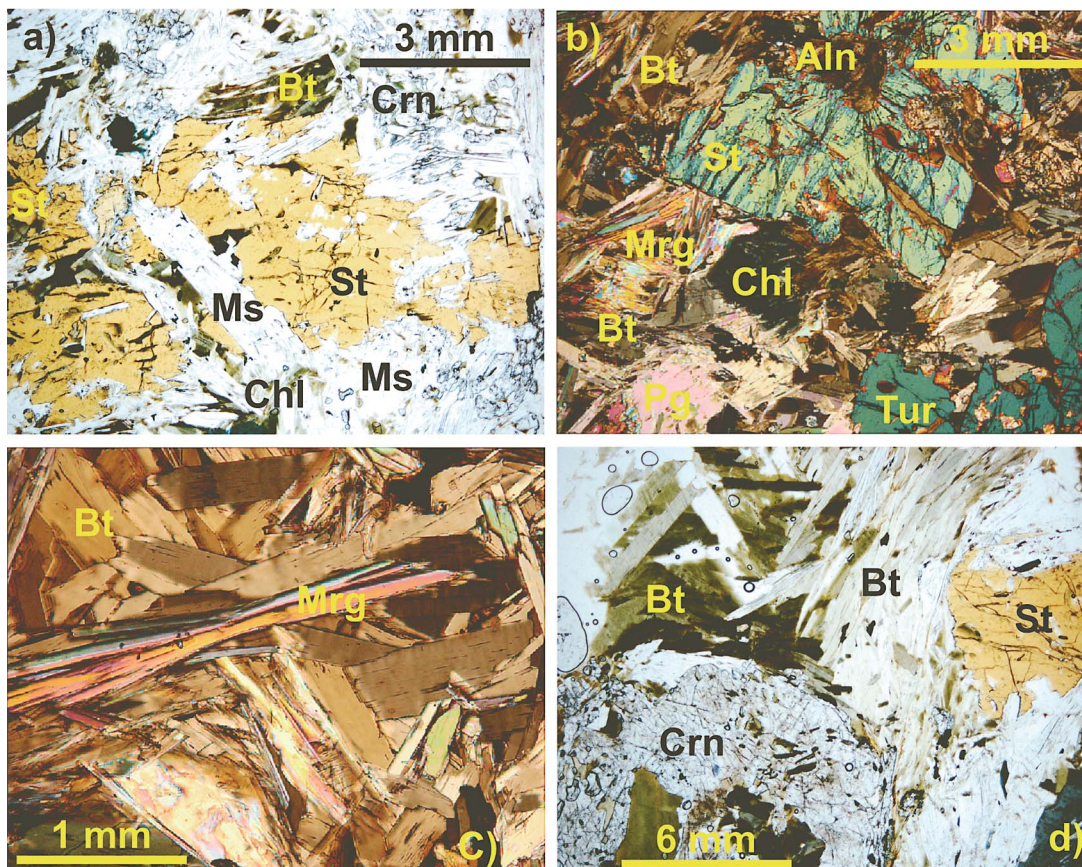


FIG. 7. Photomicrographs of textures in blackwall rocks: a) resorbed staurolite replaced by corundum, KB1002; b) expansion cracks around epidote–allanite inclusion in staurolite associated with micas and tourmaline, KB298; c) margarite blades in biotite matrix, KB298; d) very coarse corundum with biotite and relict staurolite, KB299.

respectively) appears to be mainly present in apatite (with ~1% F), biotite, tourmaline, and metamorphic monazite (X-ray composition mapping data) rather than in the white micas, where F is below detection limit.

MINERALOGICAL COMPOSITION OF THE BLACKWALL ROCKS

Mineral compositions from the Kvesjøen blackwall (Tables 3–6) were determined using a Cameca SX100 electron microprobe with internal PAP correction (Pouchou & Pichoir 1984) at IMPG, Freiburg. CAMECA-supplied natural and synthetic standards were used for most of the major and minor elements. Measuring times per element were 20 seconds with an emission current of 10 nA and an acceleration voltage of 15 kV. Alkali loss was minimized by increasing the beam size to 5 μm where possible. Back-scattered electron imaging (BEI) also was used to identify very

fine-grained accessory minerals, fine-scale mineral heterogeneity and to investigate alteration products and retrograde minerals.

The white micas

Compositions of the three coexisting white micas is shown in the KNC projection in Figure 10. Detailed compositional features (Figs. 11, 12 and 13) are presented below.

Margarite, the brittle Ca-mica, contains variable amounts of the paragonite component (22.8–34.4%) (Table 3); the muscovite content is very minor (0.2 to 1.2%), and lower in sodium-rich (>2.2% Na_2O) grains. Margarite contains between 0.72 and 0.97% SrO, and where measured, BaO is <0.10%.

Paragonite has a relatively variable composition (Table 3). Where intergrown with muscovite, it has an elevated muscovite component (>13.3%), contains mod-

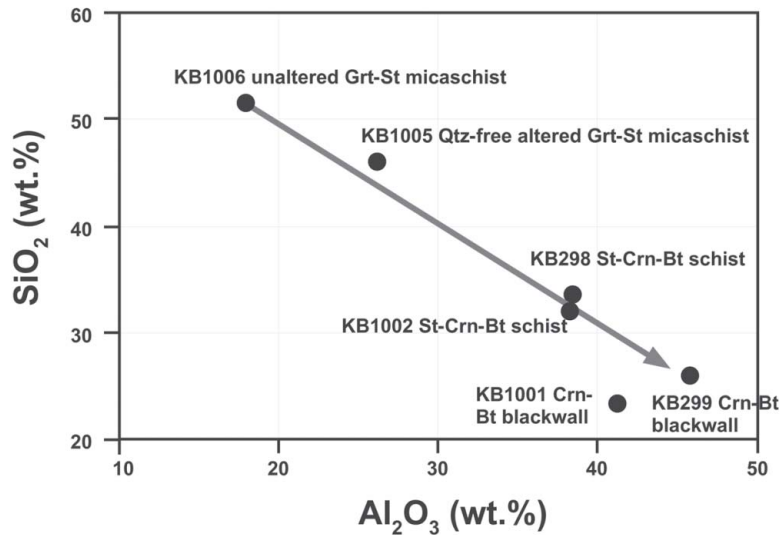


FIG. 8. Variation of bulk rock SiO_2 versus Al_2O_3 for mica schist KB1006, altered mica schist KB1005 and blackwall rocks. The arrow indicates the evolving bulk-rock composition associated with alteration of mica schist and formation of blackwall rocks.

erate amounts of margarite component (4.5 to 15.5%) and is rich in Ca where coexisting with margarite. Values of X_{Fe} vary between 0.74 and 0.81, and TiO_2 is moderately high at 0.14–0.30 wt.%. Barium is low (0.1–0.5 wt.%), and SrO ranges between 0.0 and 0.53%.

Muscovite in the blackwall rocks has a small phengite component, ranging between 7 and 8% (Table 3). The paragonite content is between 27.3 and 31.8 mol.%. This extremely high Na-content of muscovite coexisting with paragonite in the corundum-bearing rocks greatly exceeds that of the maximum paragonite content of muscovite defined by the paragonite–muscovite solvus in rocks with excess quartz and aluminosilicate. Although little is known about the paragonite–muscovite solvus at corundum saturation, the sodic muscovite grains probably reflect a metastable product of the early decomposition of primary paragonite originally present in the mica schist (see section on modeling below). Compositional disequilibrium in some white mica assemblages is indicated by inhomogeneous replacement textures (Fig. 11). In muscovite, X_{Fe} , in the range 0.54–0.65, is invariably higher than in the coexisting biotite. Titanium varies between 0.40 and 0.76 wt.%, and MnO is less than 0.02% and mostly below the detection limit. The most notable feature of the muscovite is the high and variable Ba content, between 0.78 and 4.03 wt.% BaO. It is irregularly distributed within grains. Muscovite of the staurolite–garnet mica schist protolith does not contain more than trace amounts of Ba.

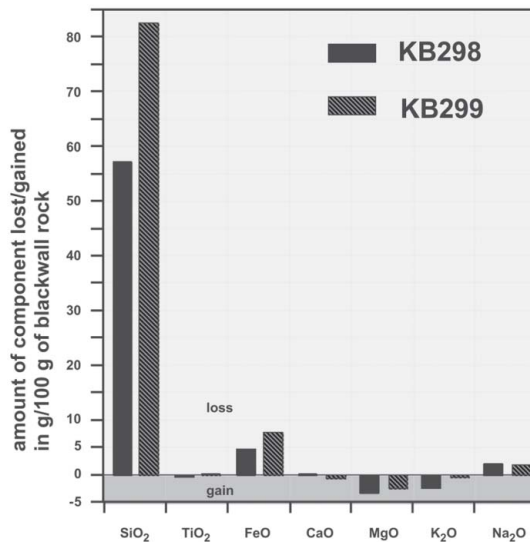


FIG. 9. Element gain and loss of blackwall samples based on normalization of the composition of the mica schist to the Al content of blackwall sample KB299.

The distribution of interlayer elements K, Na, Ca, Ba, Sr in the three micas is shown as element-concentration maps in Figures 12 and 13. Figure 12 shows the distribution in a heterogeneous grain of mica associated

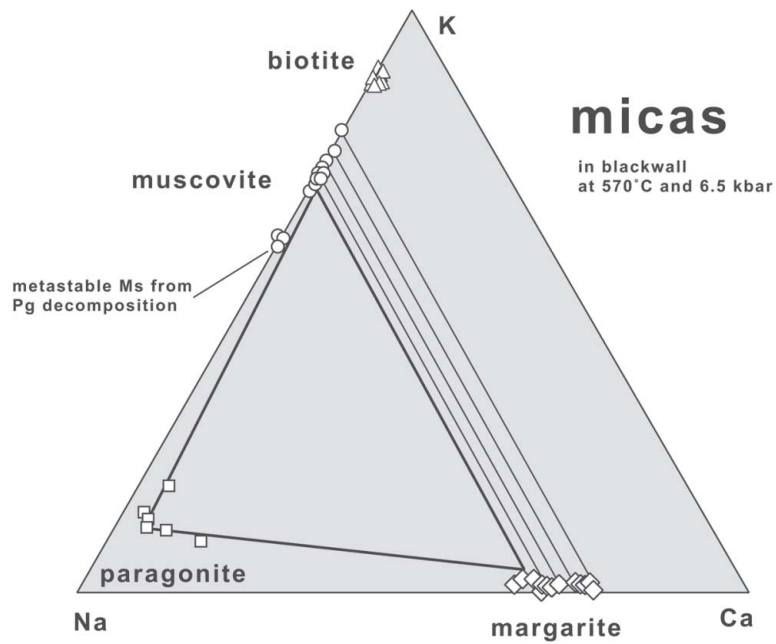


FIG. 10. KNC projection of compositions of coexisting white micas in blackwall rocks.

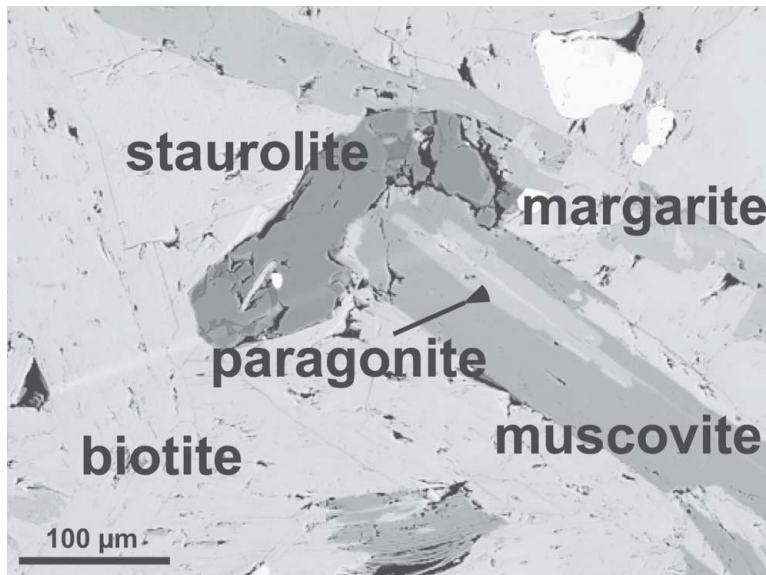


FIG. 11. Back-scattered electron image (BEI) of texture involving three micas Mrg-Pg-Ms (KB299).

with kyanite, staurolite and rutile in blackwall sample KB298. The texture indicates that paragonite is being replaced by muscovite. The paragonite contains ~0.4% CaO, and the Ca image shows an irregular distribution of Ca throughout the replacement muscovite (containing between 0.01 and 0.04% CaO) suggesting that except for the margarite, the entire grain was originally paragonite. This is also suggested by the distribution of Na, the replacement muscovite containing between 1.77 and 2.18% Na₂O. Barium is strongly partitioned into the muscovite at 1.5–2.1% BaO, with the brightest part of the grain containing 3.9% Ba. The margarite and relict paragonite contain less than 0.14% BaO. Strontium is mainly enriched in margarite (0.8–1.0% SrO) and paragonite (~0.5% SrO), with muscovite containing

between 0.27 and 0.29% SrO. Figure 12 shows the distribution of interlayer cations in a composite muscovite–margarite grain coexisting with biotite. Of interest is the irregular distribution of Ba in the muscovite, the darkest gray areas containing the least Ba, and highest K and Na. In contrast to muscovite, biotite shows a homogeneous distribution of Ba.

Biotite

The blackwall rocks contain abundant biotite. In terms of Fe–Mg content, the biotite is rather homogeneous, with X_{Fe} between 0.35 and 0.42. TiO₂ is low (1.34–1.88 wt.%), but presumably at saturation levels in the presence of ilmenite and rutile, and MnO is less

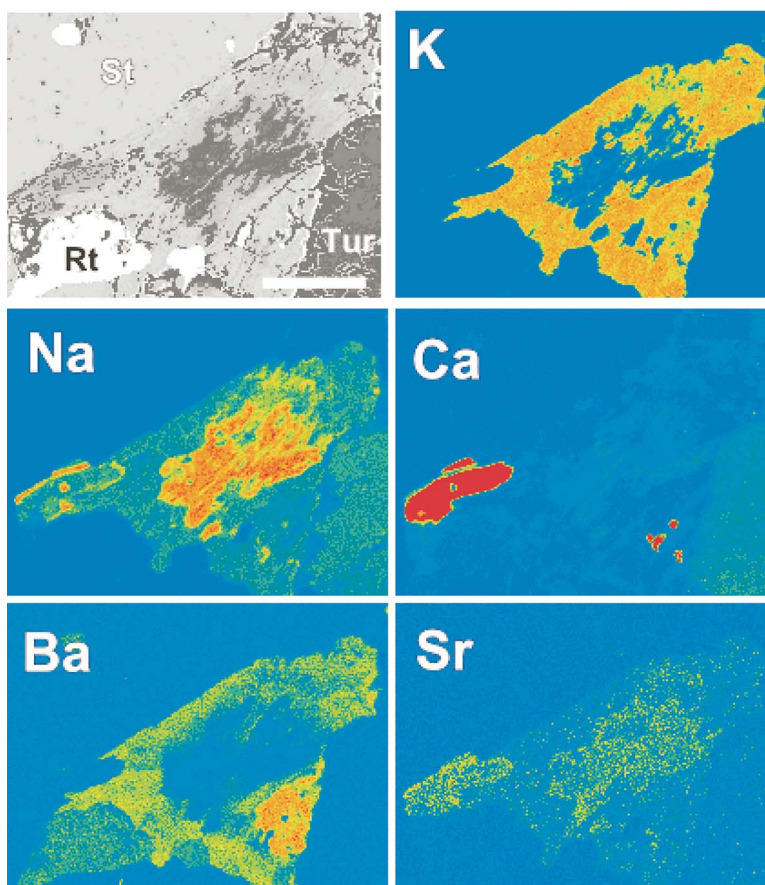


FIG. 12. BEI and K, Na, Ca, Ba, and Sr composition maps of a composite muscovite, paragonite, margarite grain in blackwall sample KB298. Associated minerals are staurolite (St), tourmaline (Tur), and rutile (Rt, white grains). The patchy nature of the paragonite, which contains ~0.40% CaO, indicates that it is being replaced by muscovite (which contains between 1.58 and 2.18% Na₂O). Area of highest Ba concentration in the muscovite contains 3.79%. The less bright areas contain between 1.46 and 2.08% BaO. Bar scale: 200 μm .

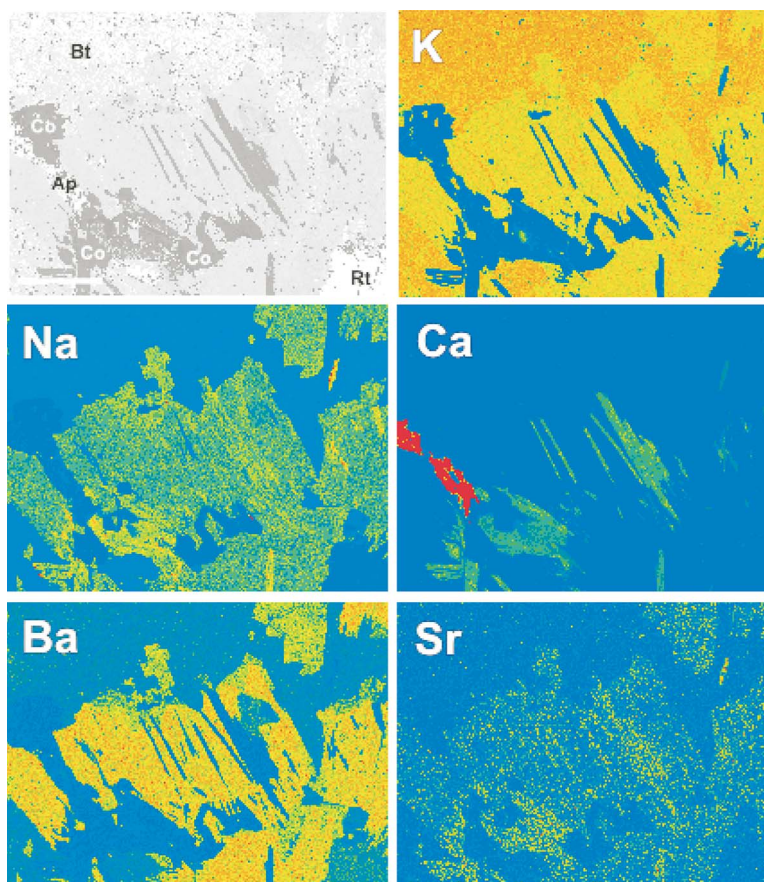


FIG. 13. BEI and K, Na, Ca, Ba, Sr composition maps of a composite muscovite – margarite grain and associated minerals in blackwall sample KB298. Bt: biotite, Co: corundum, Ap: apatite, and Rt: rutile. Muscovite contains between 2.20 and 1.58% Na_2O . The margarite contains between 2.05 and 2.25% Na_2O . The Ba content of the muscovite ranges between 0.72 and 2.08% BaO. Bar scale: 200 μm .

than 0.10 wt.% (Table 4). With VIAl between 0.80 and 1.07, biotite compositions are typical of amphibolite-grade muscovite- and Al-silicate-bearing pelites (*e.g.*, Guidotti 1984). The biotite contains significant Ba (0.82–2.47 wt.% BaO) that may show, in the absence of muscovite, a patchy zonation in individual grains, as that shown by Ti. Deficiencies in the octahedral sites are between 5.78 and 5.92 atoms per formula unit (*apfu*) (Table 4). Since 40% of the mode of KB299 is biotite, most of the bulk-rock Ba (4914 ppm, Table 2) is stored in biotite.

Staurolite

Staurolite (Table 5) has a low X_{Fe} in the range 0.73–0.78 and reflects the Mg-rich bulk composition. It contains inclusions of biotite, corroded kyanite, rutile,

monazite, epidote–allanite and, rarely, tourmaline. Staurolite of the mica schist protolith is significantly more ferrous (Fig. 5b). Staurolite of the blackwall rocks coexists with a more magnesian biotite (Fig. 5b) compared to the mica schist (Fig. 5a).

Tourmaline

Tourmaline (Table 6) occurs as porphyroblasts in both blackwall samples. As expected, compositions plot within the field of aluminous metapelite–psammite rocks defined by Henry & Guidotti (1985) in terms of their Al–Fe–Mg content. No zoning has been detected in the main part of the grains, but inclusion-free rims are slightly enriched in Mg, Na and depleted in Fe, Ca. In KB298, back-scattered electron images indicate that the tourmaline has largely overgrown the mica (*i.e.*,

muscovite ± paragonite) in the matrix and, except for a narrow inclusion-free rim, contains abundant inclusions of partly reacted margarite, fine-grained kyanite, biotite

and rare muscovite. In contrast, the tourmaline in KB299 contains abundant inclusions of biotite.

Corundum

Corundum is chemically homogeneous, with small amounts of Fe (0.44–1.28 wt.% Fe₂O₃) and Ti (<0.6 wt.% TiO₂). It commonly has a dusty appearance, being characterized by reddish patches due to the presence of fine (? exsolved) hematite (Fig. 7d).

Kyanite

Whereas small amounts of resorbed kyanite are present as inclusions in staurolite, tourmaline and muscovite, in KB298 it also forms larger grains intergrown with muscovite and biotite. The kyanite contains up to 1% Fe₂O₃ and <0.01% Cr₂O₃, MnO, Na₂O, K₂O and CaO.

Rutile

Rutile occurs as disseminated grains (typically <100 μm) and is also commonly associated with ilmenite. It typically contains less than 0.7 wt.% FeO and rarely shows fine exsolution-induced lamellae of ilmenite.

TABLE 4. COMPOSITION OF BIOTITE IN BLACKWALL SAMPLE KB299

	1	2	5	6	7	11	12	13	17	18
SiO ₂ wt. %	35.89	35.74	35.39	36.04	34.86	35.93	34.98	34.66	35.38	34.91
TiO ₂	1.64	1.64	1.52	1.34	1.52	1.74	1.76	1.56	1.80	1.88
Al ₂ O ₃	20.70	20.31	20.85	21.47	19.98	19.89	20.36	20.80	19.80	21.01
FeO	14.30	14.22	15.31	13.59	13.88	15.00	15.66	13.56	15.14	14.84
MnO	0.09	0.02	0.03	0.05	0.03	0.08	0.05	0.05	0.10	0.10
MgO	13.17	12.72	13.44	14.18	13.95	12.62	12.62	13.03	12.01	11.70
CaO	n.d.	0.01	n.d.	0.01	0.02	0.05	0.04	0.01	0.01	n.d.
Na ₂ O	0.66	0.65	0.60	0.66	0.65	0.60	0.58	0.69	0.70	0.68
K ₂ O	8.40	8.18	8.08	7.64	8.67	7.10	7.53	8.35	7.69	6.85
BaO	n.d.	n.d.	0.82	0.89	0.91	1.28	1.31	1.51	1.85	2.47
Total	94.85	93.49	96.04	95.87	94.47	94.29	94.89	94.22	94.48	94.44
Si <i>apfu</i>	5.32	5.36	5.24	5.28	5.25	5.40	5.27	5.25	5.38	5.31
^{IV} Al	2.68	2.64	2.76	2.72	2.75	2.60	2.73	2.75	2.62	2.69
^{VI} Al	0.93	0.96	0.88	0.99	0.80	0.93	0.89	0.96	0.92	1.07
Ti	0.18	0.19	0.17	0.15	0.17	0.20	0.20	0.18	0.21	0.21
Fe	1.77	1.78	1.90	1.67	1.75	1.89	1.97	1.72	1.92	1.89
Mn	0.01	0.00	0.00	0.01	0.00	0.01	0.01	0.01	0.01	0.01
Mg	2.91	2.85	2.97	3.10	3.14	2.83	2.84	2.94	2.72	2.65
Ca	0.00	0.00	0.00	0.00	0.00	0.01	0.01	0.00	0.00	0.00
Na	0.19	0.19	0.17	0.19	0.19	0.17	0.17	0.20	0.21	0.20
K	1.59	1.57	1.53	1.43	1.67	1.36	1.45	1.61	1.49	1.33
Ba	0.00	0.00	0.05	0.05	0.05	0.08	0.08	0.09	0.11	0.15
X _{Fe}	0.38	0.39	0.39	0.35	0.36	0.40	0.41	0.37	0.41	0.42
Ca mol. %	0.00	0.09	0.00	0.10	0.17	0.52	0.40	0.09	0.10	0.00
Na	10.67	10.77	10.14	11.59	10.21	11.32	10.44	11.15	12.14	13.11
K	89.33	89.14	89.86	88.31	89.62	88.16	89.16	88.76	87.76	86.89

Trace Cr₂O₃, ZnO, Cl (0.04–0.05%); n.d.: not detected, X_{Fe} = Fe/(Fe + Mg). Cation proportions, in atoms per formula unit (*apfu*), are calculated on the basis of 22 atoms of oxygen.

TABLE 5. COMPOSITION OF STAUROLITE IN BLACKWALL SAMPLE KB299

	1	2	3	4	5
SiO ₂ wt. %	27.59	27.93	27.46	27.69	27.82
TiO ₂	0.51	0.48	0.59	0.55	0.59
Al ₂ O ₃	54.01	54.16	54.18	54.13	54.25
FeO	13.44	13.53	13.38	13.75	13.10
MnO	0.20	0.23	0.37	0.32	0.17
MgO	2.47	2.43	2.19	2.21	2.69
ZnO	0.20	0.26	0.22	0.28	0.27
Total	98.28	98.82	98.23	98.69	98.73
Si <i>apfu</i>	7.61	7.66	7.58	7.61	7.62
^{IV} Al	0.39	0.34	0.42	0.39	0.38
^{VI} Al	17.17	17.17	17.21	17.16	17.15
Ti	0.11	0.10	0.12	0.11	0.12
Fe	3.10	3.10	3.09	3.16	3.00
Mn	0.05	0.05	0.09	0.07	0.04
Mg	1.02	0.99	0.90	0.91	1.10
Zn	0.04	0.05	0.04	0.06	0.05
X _{Fe}	0.75	0.76	0.77	0.78	0.73

Total includes traces of Cr, Ca, Na and K. The proportion of cations, in atoms per formula unit (*apfu*), is calculated on the basis of 46 atoms of oxygen.

TABLE 6. COMPOSITION OF TOURMALINE* IN BLACKWALL SAMPLE KB299

	1	2	3	4	5	6	7	8
SiO ₂ wt. %	34.97	35.27	35.36	35.10	35.23	34.82	34.88	35.60
TiO ₂	0.74	0.66	0.62	0.77	0.58	0.67	0.61	0.52
Al ₂ O ₃	33.31	33.14	33.22	33.07	33.12	33.23	33.30	33.46
B ₂ O ₃	10.43	9.38	10.44	9.74	10.78	10.39	10.24	10.82
FeO**	6.72	6.65	6.26	6.66	6.22	6.69	6.06	5.32
MgO	7.46	7.55	7.69	7.53	7.71	7.51	7.81	8.25
CaO	1.53	1.44	1.30	1.44	1.42	1.42	1.34	0.93
Na ₂ O	1.75	1.85	1.90	1.67	1.88	1.77	1.93	2.24
Total	96.91	95.94	96.79	95.98	96.94	96.50	96.17	97.19
Si <i>apfu</i>	5.72	5.76	5.77	5.75	5.77	5.72	5.72	5.79
Al	6.42	6.38	6.40	6.39	6.39	6.43	6.44	6.42
B	2.96	2.96	2.96	2.97	2.97	2.97	2.97	2.95
Ti	0.09	0.08	0.08	0.09	0.07	0.08	0.08	0.06
Fe	0.92	0.91	0.85	0.91	0.85	0.92	0.83	0.72
Mg	1.82	1.84	1.87	1.84	1.88	1.84	1.91	2.00
Ca	0.27	0.25	0.23	0.25	0.25	0.25	0.24	0.16
Na	0.55	0.59	0.60	0.53	0.60	0.56	0.61	0.71
X _{Fe}	0.34	0.33	0.31	0.33	0.31	0.33	0.30	0.27
X _{Ca}	0.33	0.30	0.27	0.32	0.29	0.31	0.28	0.19

* Spot analyses within a single, essentially unzoned porphyroblast. Compositions 7 and 8 pertain to the inclusion-free rim. ** All iron as FeO. Total includes traces of Cr, Mn, K. The proportion of cations, in atoms per formula unit (*apfu*), is based on 29 atoms of oxygen.

Ilmenite

Ilmenite grains are homogeneous and contain ~1% MnO, small amounts of ZnO (0.13–0.25 wt.%), and ~10.5 mol.% of the hematite component. They generally contain inclusions of ferrian rutile, and some grains show evidence of high-temperature oxidation to hematite and rutile.

Epidote-allanite

Composite epidote-allanite intergrowths occur within the mica matrix, surrounding ilmenite and as inclusions containing metamorphic monazite in staurolite and corundum. Radial cracks due to expansion around the inclusions are the result of the breakdown of cores of monazite (Fig. 7b); this topic will be the subject of a separate contribution (see Grapes *et al.* 2002).

P-T CONDITIONS OF BLACKWALL FORMATION

Mica schists

The P-T conditions of regional Caledonian metamorphism can be deduced by thermobarometry of the

TABLE 7. COMPOSITION OF MINERALS IN MICA SCHIST SAMPLE KB1006

	St	St	Grt c	Grt r	Bt	Bt	Hbl	Chl	Pl
SiO ₂ wt.%	27.40	27.39	37.16	37.00	37.68	37.57	42.41	26.06	61.46
TiO ₂	0.66	0.59	0.05	0.03	1.49	1.52	0.51	0.10	0.00
Al ₂ O ₃	52.38	51.91	21.43	21.58	18.34	18.52	16.99	22.42	24.28
FeO	9.57	9.03	31.33	31.86	13.90	14.12	13.55	17.35	
MnO	0.10	0.10	2.24	1.29	0.06	0.01	0.13	0.06	0.01
MgO	2.19	2.02	5.45	5.58	14.58	14.63	10.43	21.24	0.00
ZnO	5.74	5.75			0.14	0.15	0.09	0.06	
CaO	0.00	0.02	2.76	2.88	0.12	0.10	10.43	0.03	5.05
Na ₂ O	0.13	0.14	0.05	0.01	0.41	0.40	2.02	0.00	8.89
K ₂ O	0.00	0.02	0.00	0.00	8.52	8.76	0.36	0.00	0.07
Total	98.26	97.04	100.47	100.23	95.24	95.78	96.93	87.37	99.78
Si <i>apfu</i>	7.675	7.749	2.943	2.934	5.545	5.511	6.250	5.277	10.929
^{IV} Al	0.325	0.251			2.455	2.489	1.750	2.723	5.089
^{VI} Al	16.963	17.060	2.004	2.017	0.726	0.713	1.202	2.628	
Fe ²⁺	2.242	2.137	2.075	2.113	1.711	1.732	1.670	2.938	
Mn	0.024	0.024	0.150	0.087	0.008	0.001	0.016	0.010	0.002
Mg	0.914	0.852	0.643	0.660	3.198	3.199	2.292	6.412	
Zn	1.187	1.201			0.015	0.016	0.010	0.009	
Ti	0.139	0.126	0.003	0.002	0.165	0.168	0.057	0.015	
Ca	0.006	0.234	0.245	0.019	0.016	1.647	0.007	0.962	
Na	0.071	0.077	0.008	0.002	0.117	0.114	0.577	3.065	
K		0.007			1.599	1.639	0.068	0.016	
X _{Mg}	0.29	0.29	0.24		0.65	0.65	0.58	0.69	
An								23.8	

The total includes trace of Fe₂O₃ and Cr₂O₃. Staurolite: homogeneous Zn-rich grains. Garnet: weakly zoned to a (Fe,Mg,Ca)-rich and Mn-poor rim, inclusions of quartz common. Plagioclase, hornblende, biotite: homogeneous grains. Chlorite: interleaved with biotite. Accessories include composite monazite-apatite grains mantled by highly zoned allanite - REE-enriched epidote; apatite, zircon, rutile, significant chalcocyanite and pyrite also are present. Electron-microprobe data. The proportion of cations, in atoms per formula unit (*apfu*), is calculated on the following numbers of oxygen atoms: staurolite 46, garnet 12, biotite 22, hornblende 23, chlorite 28, and plagioclase 32. Mineral symbols are those of Kretz (1983). Abbreviations: c core, r rim.

mica schists. The assemblage of the type sample KB1006 (locality A, Fig. 3) and the mineral-composition data in Table 7 have been used together with the program GTB (Spear & Kohn 1999) to compute the following equilibria: Grt-Bt Fe-Mg exchange (Ferry & Spear 1978; Grt solution model: Berman 1990); Grt-Hbl Fe-Mg exchange (Perchuk *et al.* 1985); Hbl-Pl (Holland & Blundy 1994); Grt-Pl-Hbl-Qtz (Kohn & Spear 1989). The calibrations indicate 570° ± 20°C and 6.6 ± 0.2 kbar for equilibrium of the assemblage Grt-Bt-Hbl-Chl-St-Ep-Pl-Qtz in the mica schist, and reflect the P-T conditions of regional metamorphism in the Seve Nappes during the Scandian main phase of the Caledonian orogeny in the Silurian.

The bulk composition of the mica schist (Table 1) has been used to calculate stability relations of the assemblages (Fig. 14) using the data of Berman (1988, 1990) and Mäder *et al.* (1994) and the DOMINO-THERIAK software of de Capitani & Brown (1987). Two representative assemblages are highlighted. At P ≈ 6 kbar, the observed quartz-excess assemblage Grt-Bt-St-Pl-Chl-Mt and the alternative assemblage at slightly lower grade, Grt-Chl-Pl-Ms-Ep, indicate about 570°C for the temperature conditions of regional metamorphism. The model fails to predict the small amount of hornblende present in KB1006. The pressure is poorly constrained by the assemblages of the mica schists. However, the presence of kyanite in metasomatically altered mica schist in the blackwall zone (KB1005) constrains the P conditions to 5–7.5 kbar (Fig. 14). A pressure of 6.5 kbar is assumed for the blackwall-forming process, consistent with the Grt-Pl-Hbl-Qtz barometry above (Kohn & Spear 1989).

The sample of altered intermediate quartz-free mica schist (KB1005) is not well suited for thermobarometry because it lacks quartz. The mineral-composition data in Table 8 can be used, however, to calculate Fe-Mg exchange temperatures from the Bt-Grt and Grt-Hbl thermometers used above. The temperatures are consistent with those derived for the unaltered mica schist.

Blackwall rocks

The P-T conditions under which the blackwall rocks formed are difficult to estimate using conventional thermobarometry. The presence of three dioctahedral micas, margarite, paragonite and muscovite, suggests that they formed at temperatures below *ca.* 600°C (Hewitt & Wones 1984). At 6.5 kbar, the upper limit of margarite is at about 600°C (Guggenheim 1984).

The bulk compositions of the two blackwall samples KB298 and KB299 (Table 1) have been used to calculate the stability relations of the assemblage using the same data and code as for Figure 14. For sample KB299, the model predicts the stable assemblage Bt-Crn-St-Mrg-Pg-Chl at 570°C and 6.5 kbar (Fig. 15). Predicted modes of 40% biotite and 20% corundum are in good agreement with the observed abundances in the rock.

TABLE 8. COMPOSITIONS OF MINERALS IN ALTERED QUARTZ-FREE MICA SCHIST SAMPLE KB1005

	St	St	Ky	Grt c	Grt r	Pl c	Pl r	Pl r	Pl sym	Kfs v	Kfs	Bt	Bt	Bt	Bt sym	Pg	Hal ¹	Hbl	Hbl	Ep ²	
SiO ₂ wt.%	27.06	27.57	37.10	37.45	37.33	59.31	60.67	61.67	60.33	63.80	64.40	37.14	37.68	37.36	37.19	45.60	44.11	40.92	40.09	35.98	
TiO ₂	0.74	0.65	0.01	0.09	0.03	0.01	0.01	0.00	0.03	0.01	0.02	1.65	1.69	1.67	1.47	0.20	0.02	0.57	0.60	0.08	
Al ₂ O ₃	52.86	53.10	63.03	21.68	21.51	25.63	24.82	24.51	24.72	18.53	18.47	18.72	19.24	19.11	18.57	40.12	36.57	17.56	18.13	26.84	
Fe ₂ O ₃			0.29			0.06	0.41	0.02	0.40	0.86	0.03									7.45	
FeO	13.90	13.20		30.43	31.05							14.61	15.02	14.66	15.41	0.60	1.11	15.36	15.94		
MnO	0.05	0.06	0.02	1.82	0.75	0.05	0.02	0.01	0.00	0.00	0.02	0.01	0.02	0.01	0.02	0.00	0.02	0.11	0.06	0.03	
MgO	2.67	2.24	0.02	4.98	5.09	0.00	0.00	0.00	0.00	0.20	0.00	13.83	13.62	13.88	13.63	0.13	4.14	9.25	8.96	0.31	
ZnO	0.33	0.36	0.00									0.05	0.03	0.08	0.00	0.10	0.06	0.00		0.06	
CaO	0.00	0.01	0.00	4.70	4.44	6.59	5.54	5.46	5.58	0.29	0.00	0.03	0.00	0.00	0.02	0.84	0.21	10.05	10.04	20.92	
Na ₂ O	0.01	0.00	0.00	0.03	0.01	8.05	8.73	8.79	8.70	0.09	0.06	0.51	0.50	0.49	0.35	6.49	0.70	2.02	2.02	0.02	
K ₂ O	0.00	0.00	0.01			0.06	0.06	0.05	0.06	15.57	16.40	8.62	8.44	8.67	8.77	1.44	0.14	0.39	0.40	0.00	
Total	97.65	97.20	100.52	101.18	100.21	99.76	100.26	100.51	99.82	99.35	99.40	95.20	96.28	95.98	95.48	95.52	87.08	96.27	96.27	91.73	
Si <i>apfu</i>	7.560	7.699	0.997	2.934	2.953	10.605	10.776	10.896	10.766	11.871	11.978	5.490	5.499	5.476	5.504	5.856	3.823	6.132	6.031	2.979	
^{IV} Al	0.440	0.301				5.402	5.196	5.104	5.200	4.064	4.049	2.510	2.501	2.524	2.496	2.144	0.177	1.868	1.969		
^{VI} Al	16.967	17.178	1.996	2.002	2.006							0.752	0.809	0.777	0.743	3.929	3.559	1.233	1.246	2.620	
Fe ³⁺			0.006			0.008	0.055	0.003	0.054	0.120	0.004						0.080			0.464	
Fe ²⁺	3.248	3.083		1.954	2.054							1.806	1.823	1.797	1.907	0.064		1.925	2.006		
Mn	0.012	0.014	0.001	0.121	0.050	0.008	0.003	0.002		0.003	0.001	0.003	0.003	0.001	0.003		0.002	0.014	0.008	0.002	
Mg	1.112	0.933	0.001	0.582	0.600					0.056		3.047	2.963	3.033	3.007	0.025	0.535	2.066	2.009	0.038	
Zn	0.068	0.074										0.006	0.003	0.009		0.010	0.004			0.004	
Ti	0.156	0.137		0.005	0.002	0.001	0.001		0.004	0.001	0.003	0.183	0.186	0.184	0.164	0.019	0.001	0.064	0.068	0.005	
Ca		0.003		0.395	0.376	1.263	1.054	1.034	1.067	0.058		0.005			0.003	0.116	0.020	1.614	1.618	1.856	
Na	0.005			0.005	0.002	2.791	3.007	3.012	3.011	0.033	0.022	0.146	0.142	0.139	0.100	1.616	0.116	0.587	0.589	0.003	
K						0.014	0.014	0.011	0.014	3.696	3.891	1.626	1.572	1.621	1.656	0.236	0.016	0.075	0.077		
X _{Mg}	0.26	0.23										0.63	0.62	0.63	0.61			0.52	0.50		
An						31.1	25.9	25.5	26.1												

Notes: c: core, r: rim, v: vein, sym: symplectite, ¹Halloysite, ²Epidote on allanite; total includes trace of Cr₂O₃. Staurolite occurs as homogeneous grains; Kyanite is well-formed, no retrogression to secondary muscovite. Garnet is weakly zoned to a slightly (Fe,Mg)-rich and Mn-poor rim. Plagioclase is largely homogeneous and in some cases with a thin more Ab-rich rim; rarely in a symplectic relationship with biotite. K-feldspar forms veins and fracture fillings, particularly in hornblende. Biotite occurs as unzoned grains. Paragonite seems to be a late-stage mineral, and may be intergrown with halloysite. Hornblende occurs as unzoned grains. REE-bearing epidote forms a thin overgrowth on allanite. Accessory phases include apatite (locally in composite grains with monazite), zircon, allanite, rutile (may be rimmed by ilmenite). The proportion of cations, in atoms per formula unit (*apfu*), is calculated on the following numbers of oxygen atoms: staurolite 46, kyanite 5, garnet 12, plagioclase and K-feldspar 32, biotite and paragonite 22, halloysite 14, hornblende 23, and epidote 12.5. Electron-microprobe data.

The model also correctly predicts the presence of paragonite and margarite. However, it underestimates the mode of staurolite, and it fails to predict the presence of muscovite, which, according to Figure 11 replaces paragonite. Muscovite may be stabilized by its relatively high Na-content (1.6–2.2% Na₂O) (*e.g.*, Guidotti 1984) and possibly also by the presence of Ba (up to 3 wt.% BaO).

The agreement between the predicted assemblage and the mode of KB298 is excellent (Fig. 16) and provides confidence that the P–T estimate of ~570°C and 6.5 kbar at which blackwall formation occurred is correct. The predicted mode for KB298 is: staurolite 37%, biotite 30%, muscovite 23%, margarite and paragonite 2% each, corundum 3%, and about 1% epidote. This is in close agreement with the observed mode. The model also predicts the X_{Fe} of biotite and staurolite to be 0.3 and 0.7 respectively, identical to the values measured (Tables 3, 5).

The deduced conditions of blackwall formation coincide with the P–T estimate for the regional metamorphism. The assemblage fields of the three bulk compositions (Figs. 14–16) overlap in a narrow range of 560–580°C and 5.8–7.6 kbar.

Ultramafic rocks

The P–T estimate for mica schist and blackwall formation is also consistent with the regional metamorphic assemblages in the associated ultramafic rocks. The primary Fo–En assemblage in the ultramafic rocks requires temperatures in excess of 700°C at P ≈ 6 kbar, according to the stability diagram (Fig. 17) calculated for a typical garnet lherzolite composition. Note that the stability diagram computed is not sensitive to Ca–Al variation in the lherzolites, and typical mantle-derived lherzolite shows a restricted variability in X_{Mg}. Thus the pseudosection (Fig. 17) represents the ultramafic rocks

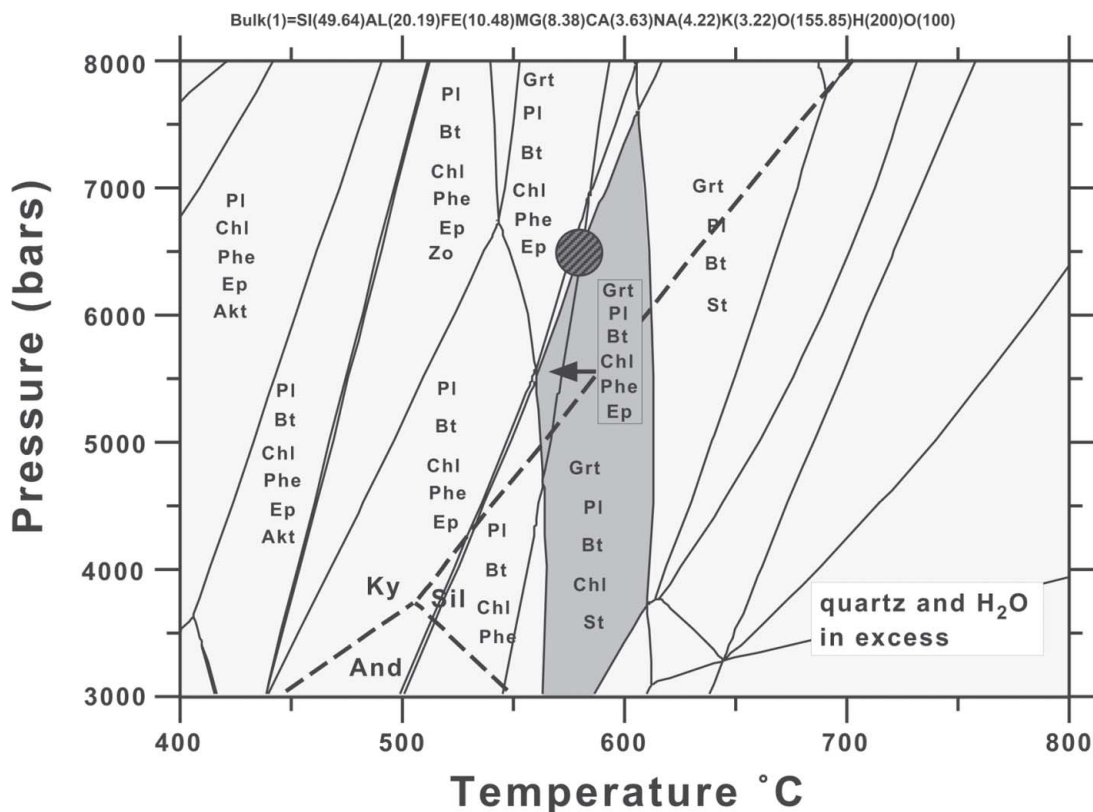
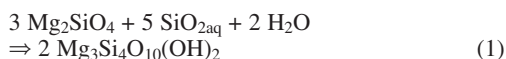


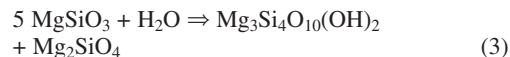
FIG. 14. Assemblage-stability diagram showing the fields of the stable phases for the composition of mica schist KB1006 (Table 1). Shaded: observed assemblages in mica schist. Dark circle: conditions during blackwall formation. Note: not all fields are labeled; for the source of the data and software, see text. Phase transitions in the aluminosilicate polymorphs are superimposed as dashed lines; data from Berman (1988).

studied. No relict anhydrous Al-minerals are present in the Kvesjöen rocks, and chlorite is the only Al-bearing phase. Tremolite carries the Ca of the rocks, as no relict clinopyroxene is present. The dominant assemblage of all ultramafic rocks in the Kvesjöen–Murusjöen area is forsterite – talc – chlorite – tremolite, which has a wide range of stability in terms of temperature (Fig. 17). Observations at outcrop and thin-section scale show that during the regional Caledonian metamorphism, the ultramafic rocks were affected by two talc-forming reactions:



In reaction (1), talc forms from forsterite, and in reaction (2), it forms from enstatite. Both talc-forming reactions

require external H_2O and SiO_2 , which is presumably derived from the surrounding rocks. Interestingly, no textural evidence for the reaction



can be found. The absence of newly formed or well-recrystallized forsterite shows that wherever an aqueous fluid was able to penetrate the ultramafic rock, it carried enough dissolved silica to produce talc from enstatite and forsterite. Talc formation in the ultramafic rocks by reactions (1) and (2) is inferred to be the pervasive process of alteration that was synchronous with blackwall formation, because talc zones at the contact to the ultramafic rocks are part of the blackwall sequence.

Theoretically, forsterite can be altered by SiO_2 metasomatism to antigorite (or other serpentine minerals),

talc, anthophyllite or enstatite. The nature of the reaction product depends on the P–T conditions under which the alteration process occurred. Talc is typical of amphibolite-facies conditions (Fig. 17). Serpentinization is conspicuously absent in nearly all ultramafic rocks of the area. Very late epitaxial overgrowth of small amounts of antigorite on chlorite is the only indication of retrograde reactions that postdate blackwall formation. Blackwall formation occurred well within the talc–forsterite field in Figure 17, consistent with the P–T estimate given above for the mica schist.

BLACKWALL FORMATION

The corundum – staurolite – biotite blackwall differs from the mica schist mainly by a much lower SiO₂ content, suggesting that silica has been the process-determining component. Hence, the first-order process of blackwall formation involves desilication of mica schist (Figs. 8, 9). The process has been modeled by a numerical mixing experiment where unaltered mica schist (KB1006) defines one end member, and the corundum –

staurolite – biotite blackwall (KB299), the other. Assemblages and modes for a series of 50 intermediate compositions have been calculated at 570°C and 6.5 kbar, and the results are shown in Figure 18. It is implicit that the removal of silica from the mica schist occurred *via* an aqueous fluid.

The alteration-progress variable ϕ along the x axis in Figure 18 is approximately equivalent to the decreasing amount of SiO₂ in the rocks toward the ultramafic body (Fig. 8) or to the time-dependent progressive loss of silica from the mica schist. At each point (step) along the reaction-progress ϕ axis, the mode of the stable assemblage is shown. It can be seen that the model predicts a continuous decrease of free quartz in the mica schist during the early stages of the alteration. Very early in the process, primary biotite and then garnet disappear. It is interesting to note that despite the notoriously refractory nature of garnet, no garnet survives in the blackwall rocks. Biotite is replaced by muscovite and chlorite.

Some major changes begin to occur when all free quartz has disappeared from the rock (at $x = 21$ in

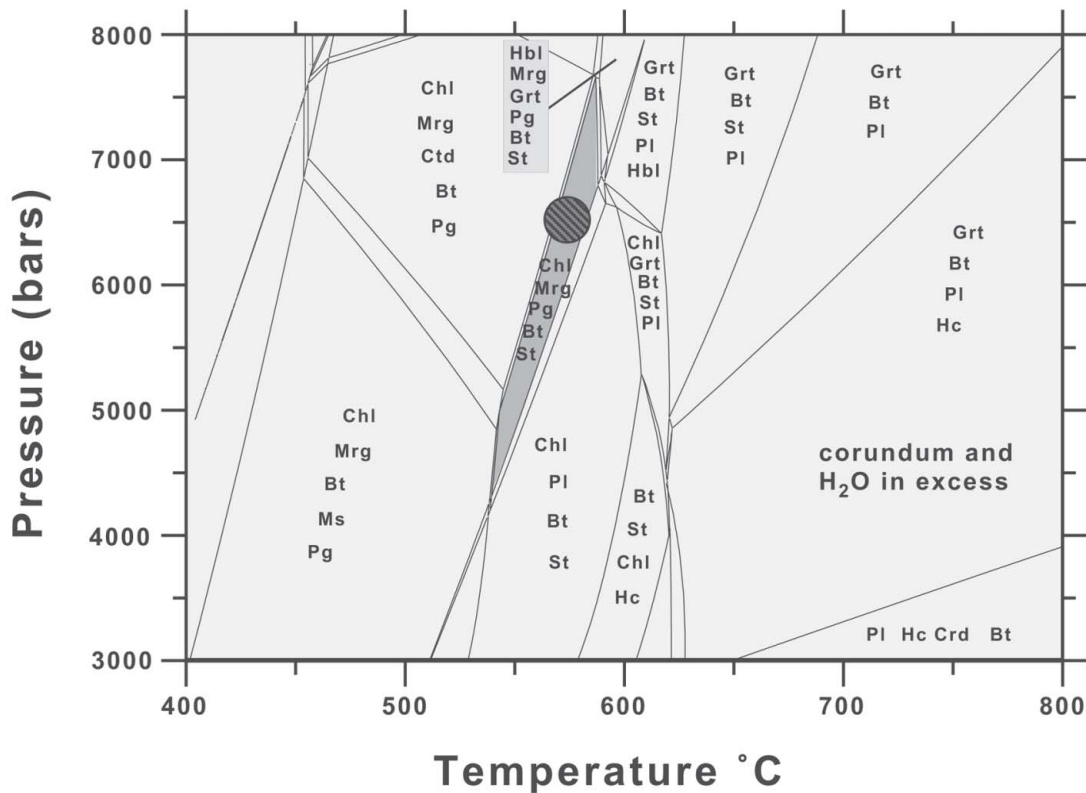


FIG. 15. Assemblage-stability diagram showing the fields of the stable phases for the composition of blackwall KB299 (Table 1). Shaded: observed assemblage of Crn–Bt blackwall. Dark circle: conditions during blackwall formation. Note: not all fields are labeled; for the source of data and software, see text.

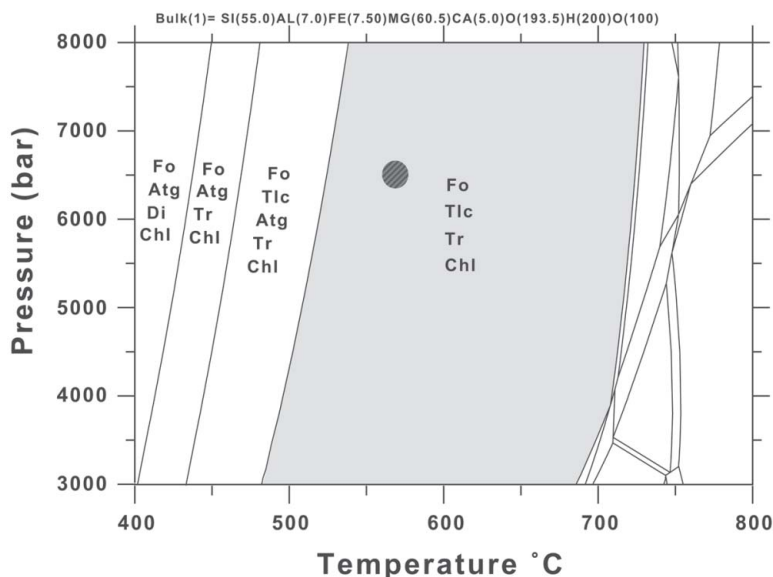


FIG. 17. Assemblage-stability diagram showing the fields of the stable phases for the composition of an average lherzolite. Shaded: observed assemblage in ultramafic rock (metalherzolite) at Storhammaren. Dark circle: conditions during blackwall formation. Note: not all fields are labeled; for the source of data and software, see text.

This reaction requires the addition of Mg from the ultramafic rock to the mica schist. A slight gain in Mg is indicated by the Al-balanced mass-conservation calculation presented above (see also Fig. 9).

The question arises as to whether the blackwall rock represents an end product of the desilication of the mica schist or an intermediate stage of an uncompleted evolution of the bulk-rock composition; is the right-hand-side of Figure 18 the ultimate blackwall and is the process completed at reaction-progress step 51? In order to answer this question, a series of mixtures has been defined by subtracting 20% of the original composition of the mica schist from the blackwall composition of KB299. The new mixing series thus extends the mixing line of Figure 18 beyond the blackwall endpoint, equivalent to decreasing the silica content of the blackwall sample KB299. The computation predicts some dramatic changes in mineralogy after further loss in silica from the blackwall. Biotite and corundum remain the dominant minerals of the rock. However, paragonite and margarite disappear abruptly, and are replaced first by zoisite and amphibole, then by nepheline, garnet and kalsilite just a few steps in desilication beyond the composition of the present-day blackwall. However, as such predicted assemblages have never been reported in any blackwall sequence, it seems likely that the corundum – staurolite – biotite blackwall very nearly represents an end-product in blackwall development. The Kvesjöen rock is thus a mature evolved blackwall and cannot be

desilicated further by peridotite. This conclusion is supported by the absence of steep gradients in the activity of SiO_2_{aq} between blackwall and ultramafic rock (see next section).

Finally, a last mixing experiment was constructed with the corundum – staurolite – biotite blackwall and the unaltered peridotite as compositional end-members, simulating the transition across the initial fault-contact between mica schist and ultramafic body. The major compositional difference of the two rocks is the high Al content in the blackwall and the high Mg content of the peridotite. The scale at which this compositional transition is observed to occur is on the order of some tens of cm (10–30 cm). A dominant feature of the numerical analysis is the development of a chlorite-rich central zone with nearly 70 vol.% chlorite (Fig. 19). Chlorite replaces corundum if the rock composition becomes increasingly more magnesian. A prominent talc-rich zone may not form in this sequence because of the high-Al environment, which favors chlorite development. Exceptionally, chlorite-rich selvages are commonly present at the outer edges of outcrops of ultramafic rocks at this metamorphic grade (lower to middle amphibolite facies) (*e.g.*, Frost 1975, Sanford 1982, Grapes & Palmer 1996), as is also the case in the Kvesjöen–Murusjöen area. Such selvages are likely to represent the location of the original fault-contact along which the ultramafic body has been emplaced into crustal rocks. As the chlorite-rich selvages are mechanically weak and

weather easily, they are generally not well preserved or exposed.

MECHANISM OF THE METASOMATIC PROCESS

What causes the quartz-rich mica schist to release SiO_2 and alter into a corundum-rich blackwall? The main driving force of the metasomatic process is the low chemical potential of SiO_2 imposed by reaction (1) in the ultramafic rocks. This stable reaction consumes silica liberated by the blackwall-forming reactions to form talc. The reaction stops when forsterite is used up. In the Storhammaren ultramafic body, forsterite is present in excess. The talc-forsterite assemblage in the ultramafic rocks buffers the activity of $\text{SiO}_{2\text{aq}}$ in the aqueous fluid; reaction (1) can be rearranged to define $a_{\text{SiO}_{2\text{aq}}}$

$$\text{SiO}_{2\text{aq}} = 0.2 (2 \text{ Tlc} - 3 \text{ Fo} - 2 \text{ H}_2\text{O}) \quad (9).$$

The actual value of $\log a_{\text{SiO}_{2\text{aq}}}$ is -1.315 using a standard state for unit activity of a hypothetical one molal solution of $\text{SiO}_{2\text{aq}}$ at infinite dilution at P and T, unit

activity of pure solids, and H_2O at P and T, and using data given by Berman (1988), Helgeson *et al.* (1981) and Walther & Helgeson (1977) and ignoring the low X_{Fe} in talc and forsterite. The silica potential in the mica schist is fixed by the presence of quartz:

$$\text{SiO}_{2\text{aq}} = \text{Qtz} \quad (10).$$

At the conditions of blackwall formation, the value of $\log a_{\text{SiO}_{2\text{aq}}}$ is -0.645 at quartz saturation (Fig. 20). If we assume activity coefficients close to unity for the uncharged silica complex in aqueous fluids (Walther & Helgeson 1977), the concentration of SiO_2 in the fluid is 2.9 g L^{-1} in the ultramafic rock and 13.6 g L^{-1} in the mica schist. The marked concentration-gradient in the fluid phase is the ultimate driving force of blackwall formation and causes migration of SiO_2 from mica schist to ultramafic rock. The consequence of silica loss from the mica schist is the formation of the corundum-staurolite-biotite blackwall modeled by a silica-loss alteration progress (Fig. 18), and the silica gain by the ultramafic rock that results in the progressive formation of talc. The concentration gradient in silica and the re-

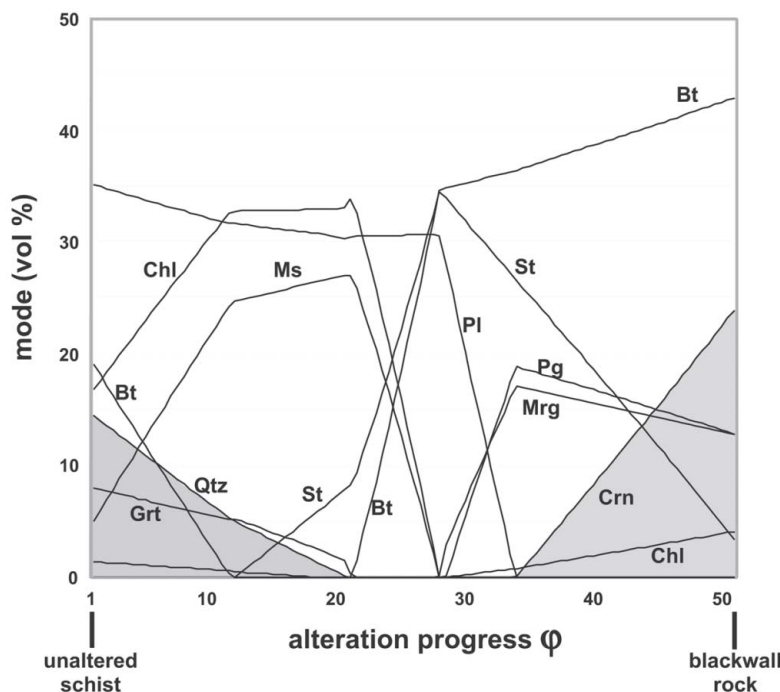


FIG. 18. Model for the development of blackwall: silica loss from mica schist is monitored by the alteration progress, which subdivides the compositional difference between mica schist KB1006 and blackwall KB299 into 50 steps. At each of the 51 rock compositions, the diagram shows the computed mode of the stable assemblage at 570°C and 6.5 kbar and excess H_2O .

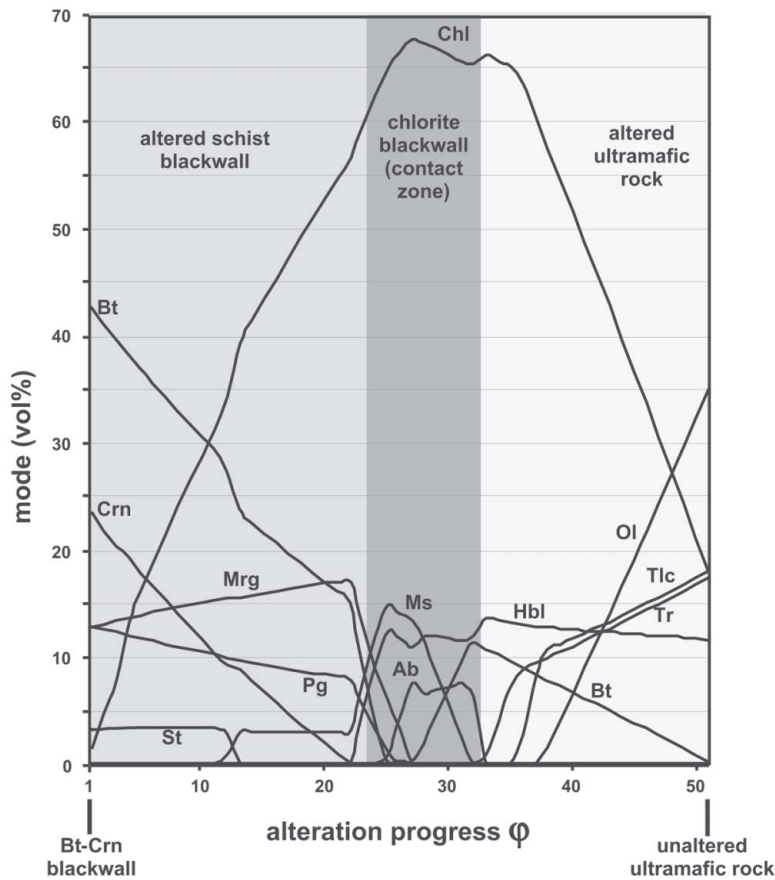
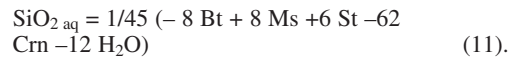


FIG. 19. Model for blackwall development: mixing of blackwall KB299 (Table 1) with ultramafic rock of typical lherzolite composition. Mixing equal amounts of each rock type at the original thrust-fault contact will result in a central zone modally dominated (70 vol.%) by chlorite (chlorite blackwall).

sultant blackwall-zonation pattern are shown in Figure 20 with distances (x axis) approximated from the variable width and somewhat poorly exposed zones. Consequently, calculated concentration-gradients (in $\text{g SiO}_2 \text{ L}^{-1} \text{ m}^{-1}$) are also somewhat imprecise. Nevertheless, it is evident that on both sides of the original fault-contact, fluids with highly contrasting concentrations of silica were present, and the mineral assemblages in the mica schist and the ultramafic body buffered $a_{\text{SiO}_2 \text{ aq}}$ so as to maintain the gradients. The difference in fluid composition between the ultramafic rock and the mica schist is about 10 g SiO_2 per liter (Fig. 20) and occurs over a distance of less than one meter at the Storhamaren locality. The central blackwall rock is also capable of constraining μ_{SiO_2} . The blackwall assemblage Bt–Ms–St–Crn buffers μ_{SiO_2} through the equilibrium:



The μ_{SiO_2} is fixed by the assemblage Bt–Ms–St–Crn at both sides of the blackwall, and there is no SiO_2 concentration gradient in the fluid across the central blackwall zone. The $\log a_{\text{SiO}_2 \text{ aq}} = -1.05$ imposed by the blackwall assemblage corresponds to $5.35 \text{ g L}^{-1} \text{ SiO}_2$ in the fluid. This is still about twice the amount that is in equilibrium with talc and forsterite in the ultramafic rock; however, it is much lower than in the mica schist. Also, it should be noted that the presence of relics of kyanite in the blackwall defines a concentration in SiO_2 of about 12 g L^{-1} owing to the metastable reaction (12):



This is much higher than that imposed by the stable assemblage Crn–Bt–Ms–St in the blackwall. Accordingly, kyanite should decompose to corundum and release silica to the fluid phase.

If the $a_{\text{SiO}_2\text{aq}}$ in the rock sequence is buffered to an equilibrium value, a configuration is expected to develop that corresponds to the heavy line in Figure 20. This configuration is characterized by plateaus of constant values, with the reaction zones containing low-variance assemblages capable of buffering SiO_2aq . In reality, the concentration profile is expected to be similar to the dashed line in Figure 20, which is a disequilibrium configuration that describes the actual process. In the mica schist, the fluid is initially undersaturated with respect to quartz, causing first quartz and then plagioclase to dissolve (dashed curve below the plateau value). Once dissolved, silica is transported along the gradient

toward the ultramafic rock or simply carried along in the advecting fluid and fixed in the ultramafic rock by reaction (1). The smoothed disequilibrium profile (Fig. 20) shows a relatively flat gradient between the corundum – biotite rock and peridotite. At the edge of the peridotite, the dashed curve is above the plateau value defined by the assemblage forsterite – talc. Silica oversaturation with respect to the stable assemblage in the ultramafic rock drives the talc-producing reaction (1) and causes the observed ubiquitous formation of talc.

CONCLUSIONS

The unique margarite-bearing corundum–biotite blackwall at the Kvesjøen locality in central Norway formed from a garnet–staurolite mica schist by a desilication process triggered by the low chemical po-

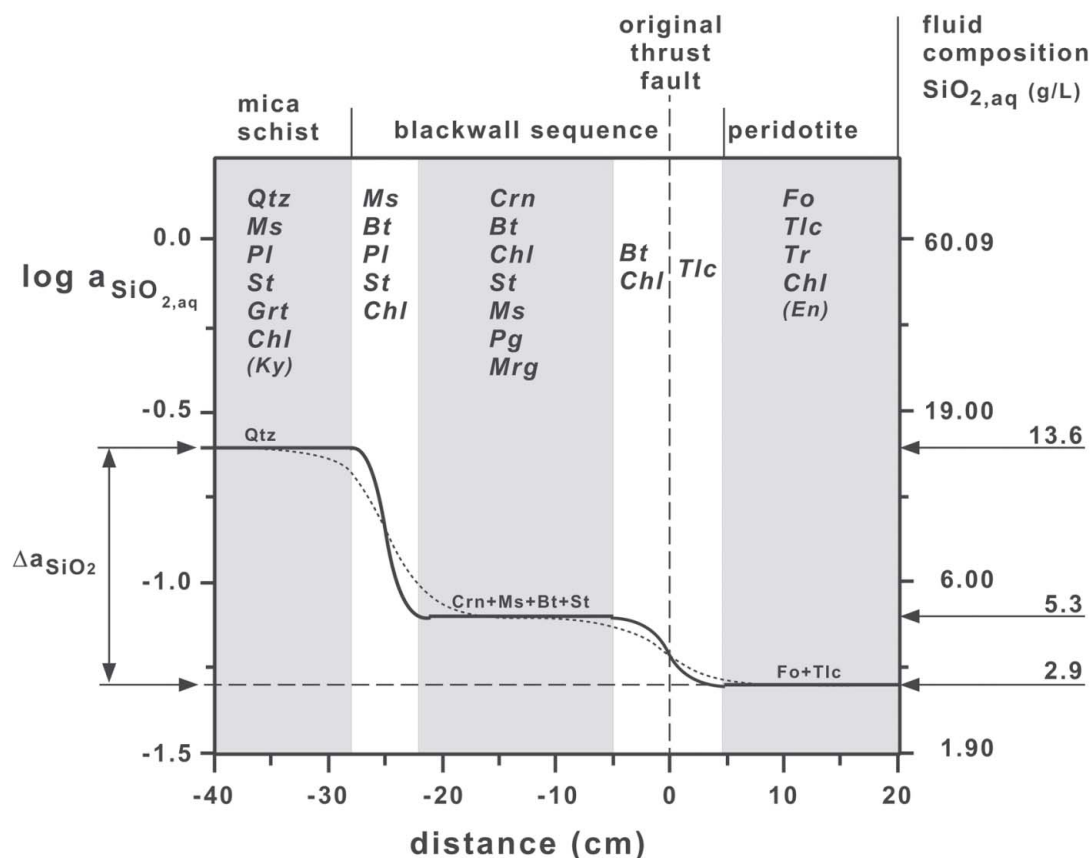


FIG. 20. Activity of SiO_2aq versus distance profile across the blackwall-alteration zone. Observed assemblages in italics, relics in brackets. The thick solid line shows the equilibrium profile buffered by mineral assemblages in the three gray shaded zones (horizontal lines are plateau concentrations; buffering assemblage given at the horizontal lines). The dotted line shows a possible real profile with disequilibrium concentrations at the edges of the plateaus leading to quartz dissolution in the mica schist and forsterite replacement by talc in the ultramafic rock, respectively. Concentrations of SiO_2 in the fluid (g L^{-1}) are shown along the right vertical axis. Δa_{SiO_2} at left vertical axis indicates the maximum difference in $\log a_{\text{SiO}_2\text{aq}}$ between mica schist and ultramafic rock. The original thrust-fault is located between the Crn–Mrg blackwall and the ultramafic rock.

tential of SiO₂ imposed by the forsterite + talc assemblage in the enclosing ultramafic rock. Results of the numerical mixing experiments presented here show that the Qtz + Pl + Bt + Grt + St + Chl + Ms assemblage of the mica schist is progressively replaced by a complex succession of new assemblages that are depleted in silica relative to the original mica schist and that buffer the chemical potential of SiO₂ to successively lower values as the desilication process progresses. Early in the process, micas, and later quartz, disappear from the mica schist. In a second stage, chlorite and secondary muscovite are consumed to form new biotite and a secondary generation of staurolite. Concurrent with feldspar breakdown, new micas are predicted to form, including margarite and paragonite (both observed). At the final stage, all earlier-formed staurolite decomposes to form corundum. The end product of this predicted complex succession of assemblages and modal changes is a margarite–corundum blackwall with the properties and modal composition of the observed blackwall. Intermediate stages of the predicted evolution of the blackwall are present at the Kvesjøen locality, and their assemblages and modes fit well the modeled process.

The nearby ultramafic rock has taken up all the silica continuously released by the mica schist *via* a reaction that formed talc from forsterite + silica in the fluid. Fluid flow is the dominant mechanism of transport of silica to the ultramafic rock.

ACKNOWLEDGEMENTS

We all thank Dugald Carmichael for inspiration and friendship. In particular, the senior author, KB, has been greatly influenced by Dugald's milestone papers on dissolution and precipitation reactions in metamorphic rocks. The basic idea in these, the conservation of Al, also is the foundation of this research communication. In addition, KB also shares delightful memories of various great field trips with Dugald Carmichael to the Alps, in Greece and to the famous Whetstone Lake in Canada.

Field work for this study was supported by the University of Oslo, Norges Forskningsrådet and the University of Freiburg. Analytical data were produced with the help of IMPG personnel, Dr. Hiltrud Müller-Sigmund (EPMA), Isolde Schmidt (XRF), Sigrid Hirth-Walter (FeO, H₂O, CO₂, C analyses), and Dr. Manfred Martin (XRF) of the Geological Survey of Baden-Württemberg, Freiburg. We thank Bob Wintsch, Rob Berman and Marc St-Onge for thoughtful reviews. Robert F. Martin and Marc St-Onge are thanked for their careful editorial handling of the manuscript.

REFERENCES

- BERMAN, R.G. (1988): Internally-consistent thermodynamic data for minerals in the system: Na₂O–K₂O–CaO–MgO–FeO–Fe₂O₃–Al₂O₃–SiO₂–TiO₂–H₂O–CO₂. *J. Petrol.* **29**, 445-522.
- BERMAN, R.G. (1990): Mixing properties of Ca–Mg–Fe–Mn garnets. *Am. Mineral.* **75**, 328-344.
- BUCHER, K. & FREY, M. (2002): *Petrogenesis of Metamorphic Rocks*. Springer-Verlag, Berlin, Germany.
- BUCHER-NURMINEN, K. (1988): Caledonian metamorphism of ultramafic rocks in the Central Scandinavian Caledonides. *Norges geologiske undersøkelse, Spec. Publ.* **3**, 86-95.
- _____ (1991): Mantle fragments in the Scandinavian Caledonides. *Tectonophysics* **190**, 173-192.
- CARMICHAEL, D.M. (1968): On the mechanism of prograde metamorphic reactions in quartz-bearing pelitic rocks. *Contrib. Mineral. Petrol.* **20**, 244-267.
- CHIDESTER, A.H. & CADY, W.M. (1972): Origin and emplacement of alpine-type ultramafic rocks. *Nature Phys. Sci.* **240**, 27-31.
- COLEMAN, R.G. (1971): Plate tectonic emplacement of upper mantle peridotites along continental edges. *J. Geophys. Res.* **76**, 1212-1222.
- COOPER, A.F. (1976): Concentrically zoned ultramafic pods from the Haast Schist zone, South Island, New Zealand. *N.Z. J. Geol. Geophys.* **19**, 603-623.
- CURTIS, C.D. & BROWN P.E. (1969): The metasomatic development of zoned ultrabasic bodies, Unst, Shetland. *Contrib. Mineral. Petrol.* **24**, 275-292.
- DE CAPITANI, C. & BROWN, T.H. (1987): The computation of chemical equilibrium in complex systems containing non-ideal solutions. *Geochim. Cosmochim. Acta* **51**, 2639-2652.
- DUBINSKA, E. & WIEWIÓRA, A. (1999): Layer silicates from a rodingite and its blackwall from Przermilów (Lower Silesia, Poland): mineralogical record of metasomatic processes during serpentinization and serpentinite recrystallization. *Mineral. Petrol.* **67**, 223-237.
- EVANS, B.W. (1977): Metamorphism of Alpine peridotite and serpentinite. *Annu. Rev. Earth Planet. Sci.* **5**, 397-447.
- FERRY, J.M. & SPEAR, F.S. (1978): Experimental calibration of the partitioning of Fe and Mg between biotite and garnet. *Contrib. Mineral. Petrol.* **66**, 113-117.
- FOSLIE, S. (1959): Nordli. *Norges Geologiske Undersøkelse, Geol. Map* **54B** (scale 1:100,000).
- FROST, B.R. (1975): Contact metamorphism of serpentinite, chlorite blackwall and rodingite at Paddy-Go-Easy pass, central Cascades, Washington. *J. Petrol.* **16**, 272-313.
- GEE, D.G., KUMPULAINEN, R., ROBERTS, D., STEPHENS, M.B., THON, A. & ZACHRISSON, E. (1985): Scandinavian Caledonides; tectonostratigraphic map. *In* The Caledonide Orogen – Scandinavia and Related Areas. (D.G. Gee & B.A. Sturt, eds.). Wiley, Chichester, U.K.

- GRAPES, R., BUCHER, K. & HOSKIN, P. (2002): Monazite stability during amphibolite grade metamorphism: corona development and element diffusion. *Beihefte Deutsche Mineral. Gesellsch.* **14**, 58 (abstr.).
- _____ & PALMER, K. (1996): (Ruby-sapphire) – chromian mica – tourmaline rocks from Westland, New Zealand. *J. Petrol.* **37**, 293-315.
- GRIFFIN, W.L. (1971): Mineral reactions at a peridotite–gneiss contact, Jotunheimen, Norway. *Mineral. Mag.* **38**, 435-445.
- GUGGENHEIM, S. (1984): The brittle micas. In *Micas* (S.W. Bailey, ed.). *Rev. Mineral.* **13**, 61-104.
- GUIDOTTI, C.V. (1984): Micas in metamorphic rocks. In *Micas* (S.W. Bailey, ed.). *Rev. Mineral.* **13**, 357-467.
- HELGESON, H.C., KIRKHAM, D.H. & FLOWERS, G.C. (1981): Theoretical prediction of the thermodynamic behavior of aqueous electrolytes at high pressures and temperatures. IV. Calculation of activity coefficients, osmotic coefficients, and apparent molal and standard and relative partial molal properties to 600°C and 5 kb. *Am. J. Sci.* **281**, 1249-1516.
- HENRY, D.J. & GUIDOTTI, C.V. (1985): Tourmaline as a petrogenetic indicator mineral: an example from the staurolite-grade metapelites of NW Maine. *Am. Mineral.* **70**, 1-15.
- HEWITT, D.A. & WONES, D.R. (1984): Experimental phase relations of the micas. In *Micas* (S.W. Bailey, ed.). *Rev. Mineral.* **13**, 201-256.
- HOLLAND, T. & BLUNDY, J. (1994): Non-ideal interactions in calcic amphiboles and their bearing on amphibole–plagioclase thermometry. *Contrib. Mineral. Petrol.* **116**, 433-447.
- KOHN, M.J. & SPEAR, F.S. (1989): Empirical calibration of geobarometers for the assemblage garnet + hornblende + plagioclase + quartz. *Am. Mineral.* **74**, 77-84.
- KOONS, P.O. (1981): A study of natural and experimental metasomatic assemblages in an ultramafic-quartzofeldspathic metasomatic system in the Haast Schist, South Island, New Zealand. *Contrib. Mineral. Petrol.* **78**, 189-195.
- KRETZ, R. (1983): Symbols for rock-forming minerals. *Am. Mineral.* **68**, 277-279.
- LOCKWOOD, J.P. (1972): Possible mechanisms for the emplacement of alpine-type serpentinite. *Geol. Soc. Am., Mem.* **132**, 273-287.
- MÄDER, U.K., PERCIVAL, J.A. & BERMAN, R.G. (1994): Thermobarometry of garnet – clinopyroxene – hornblende granulites from the Kapuskasing structural zone. *Can. J. Earth Sci.* **31**, 1134-1145.
- MATTHEWS, D.W. (1967): Zoned ultrabasic bodies in the Lewisian of the Moine Nappe in Skye. *Scot. J. Geol.* **3**, 17-33.
- PEACOCK, S.M. (1987): Serpentinization and infiltration metasomatism in the Trinity peridotite, Klamath province, northern California: implications for subduction zones. *Contrib. Mineral. Petrol.* **95**, 55-70.
- PERCHUK, L.L., ARANOVICH, L.Y., PODLESSKII, K.K., LAVRANT'eva, I.V., GERASIMOV, V.Y., FED'KIN, V.V., KITSUL, V.I., KARASAKOV, L.P. & BERDNIKOV, N.V. (1985): Precambrian granulites of the Aldan shield, eastern Siberia, USSR. *J. Metamorph. Geol.* **3**, 265-310.
- PHILLIPS, A.H. & HESS, H.H. (1936): Metamorphic differentiation at contacts between serpentine and siliceous country rock. *Am. Mineral.* **21**, 333-362.
- POUCHOU, J.L. & PICOIR, F., (1984): A new model for quantitative analysis. I. Application to the analysis of homogeneous samples. *La Recherche Aérospatiale* **3**, 13-38.
- PUSCHNIG, A.R. (2002): Metasomatic alterations at mafic-ultramafic contacts in Valmalenco (Rhetic Alps, N-Italy). *Schweiz. Mineral. Petrogr. Mitt.* **82**, 515-536.
- QVALE, H. & STIGH, J. (1984): Ultramafic rocks in the Scandinavian Caledonides. In *The Caledonide Orogen: Scandinavia and Related Areas* (D.G. Gee & B.A. Sturt, eds.). Wiley, Chichester, U.K. (693-716).
- READ, H.H. (1934): On zoned associations of antigorite, talc, actinolite, chlorite, and biotite in Unst, Shetland Island. *Mineral. Mag.* **23**, 519-540.
- ROBERTS, D. & GEE, D.G. (1985): An introduction to the structure of the Scandinavian Caledonides. The Caledonide orogen: Scandinavia and related areas. In *The Caledonide Orogen: Scandinavia and Related Areas* (D.G. Gee & B.A. Sturt, eds.). Wiley, Chichester, U.K. (55-68).
- SANFORD, R.F. (1982): Growth of ultramafic reaction zones in greenschist to amphibolite facies metamorphism. *Am. J. Sci.* **282**, 543-616.
- SHARPE, M.R. (1980): Metasomatic zonation of an ultramafic lens at Ikátoq, near Færingshavn, southern Greenland. *Grønlands Geol. Undersøgelse, Bull.*
- SIGMOND, E.M.O., GUSTAVSON, M. & ROBERTS, D. (1984): Berggrunnskart over Norge. *Norges geologiske Undersøkelse, Map* (scale 1:1 million).
- SPEAR, F.S. & KOHN, M.J. (1999): *Program Thermobarometry*, version 2.1. Available at: http://www.geo.rpi.edu/fac-staff/spear/GTP_Prog/GTP.html
- STIGH, J. & RONGE, B. (1978): Origin and emplacement of two compositional layered ultramafic bodies in the Caledonides of Västerbotten, Sweden. *Geol. Fören. Stockholm Förh.* **100**, 317-334.
- TAKLA, M.A., TROMMSDORFF, V., BASTA, F.F. & SUROUR, A.A. (2003): Margarite in ultramafic alteration zones (blackwall): a new occurrence in Barramiya area, Egypt. *Eur. J. Mineral.* **15**, 991-999.

THOMPSON, J.B., JR. (1959): Local equilibrium in metasomatic processes. *In* *Researches in Geochemistry* **2** (P.H. Abelson, ed.). John Wiley, New York, N.Y. (427-457).

WALTHER, J.V. & HELGESON, H.C. (1977): Calculation of the thermodynamic properties of aqueous silica and the solubility of quartz and its polymorphs at high pressures and temperatures. *Am. J. Sci.* **277**, 1315-1351.

WINTER, J.D. (2001): *An Introduction to Igneous and Metamorphic Petrology*. Prentice Hall, Upper Saddle River, New Jersey.

Received August 22, 2003, revised manuscript accepted November 20, 2004.